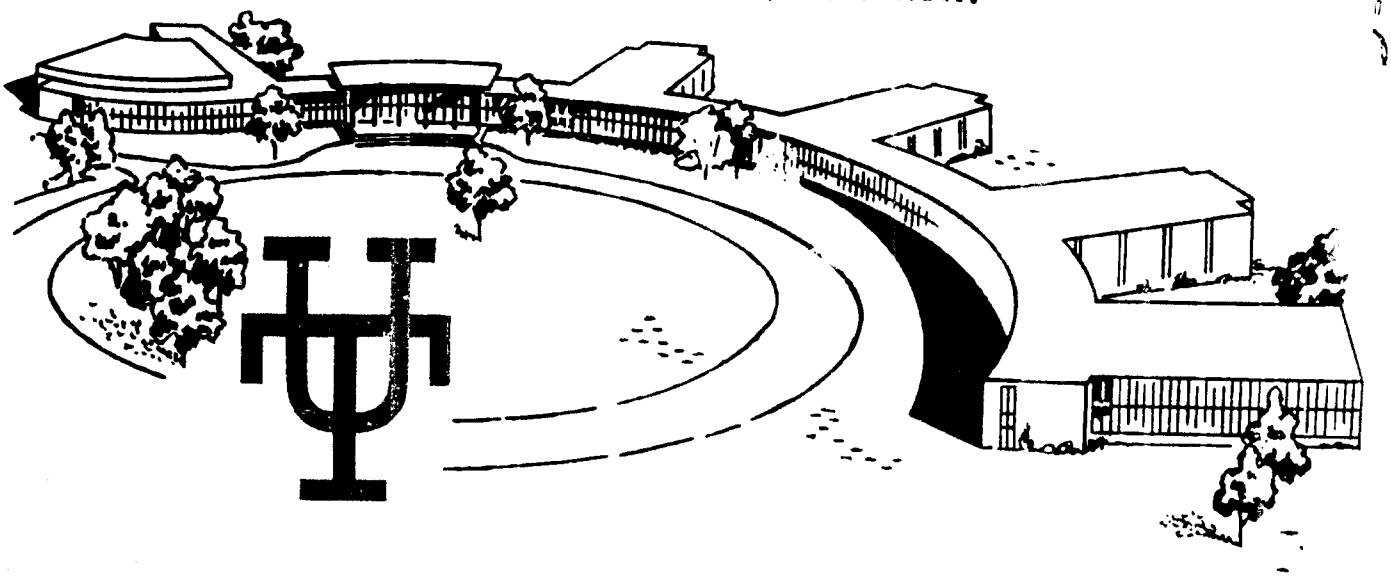

THE UNIVERSITY of TENNESSEE SPACE INSTITUTE

Tullahoma, Tennessee

DISCLAIMER NOTICE

THIS DOCUMENT IS BEST QUALITY PRACTICABLE. THE COPY FURNISHED TO DTIC CONTAINED A SIGNIFICANT NUMBER OF PAGES WHICH DO NOT REPRODUCE LEGIBLY.

UNCLASSIFIED Velocities

SECURITY CLASSIFICATION OF THIS PAGE (When Data Entered)

REPORT DOCUMENTATION PAGE	READ INSTRUCTIONS BEFORE COMPLETING FORM
1. REPORT NUMBER	2. GOVT ACCESSION NO. AD-A093 768 / 3. RECIPIENT'S CATALOG NUMBER
4. TITLE (and Subtitle) (6) Development of a Method for Predicting Trajectories and Terminal Speeds of Back-blast Debris from Small Rockets.	5. TYPE OF REPORT & PERIOD COVERED (9) Final Report May '79 — Aug 80
	6. PERFORMING ORG. REPORT NUMBER
7. AUTHOR(s) (10) Rush E. Elkins / Dennis R. Keefer	8. CONTRACT OR GRANT NUMBER(s) (15) DAAG29-79-C-0098 DAAG-29-79-C-0227
9. PERFORMING ORGANIZATION NAME AND ADDRESS University of Tennessee Space Institute Tullahoma, TN 37388	10. PROGRAM ELEMENT, PROJECT, TASK AREA & WORK UNIT NUMBERS P-16711-A-E
11. CONTROLLING OFFICE NAME AND ADDRESS U. S. Army Research Office Post Office Box 12211 Research Triangle Park, NC 27709	12. REPORT DATE (11) December 1980 13. NUMBER OF PAGES
14. MONITORING AGENCY NAME & ADDRESS (if different from Controlling Office) (12) 82	15. SECURITY CLASS. (of this report) Unclassified 15a. DECLASSIFICATION/DOWNGRADING SCHEDULE

16. DISTRIBUTION STATEMENT (of this Report)

Approved for public release; distribution unlimited.

(18) ARO (19) 16711.1-A-E

17. DISTRIBUTION STATEMENT (of the abstract entered in Block 20, if different from Report)

NA

18. SUPPLEMENTARY NOTES

The view, opinions, and/or findings contained in this report are those of the author(s) and should not be construed as an official Department of the Army position, policy, or decision, unless so designated by other documentation.

19. KEY WORDS (Continue on reverse side if necessary and identify by block number)

Antitank Ammunition, Antitank weapons, Ballistics, Debris, Explosions, Hazards, Human Factors Engineering, Rockets, Rocket Blast, Rocket Exhaust, Recoilless guns

20. ABSTRACT (Continue on reverse side if necessary and identify by block number)

See attached sheet.

DD FORM 1 JAN 73 1473 EDITION OF 1 NOV 65 IS OBSOLETE UNCLASSIFIED

SECURITY CLASSIFICATION OF THIS PAGE (When Data Entered)

387070

81 1 12 034

ABSTRACT

A semiempirical model is developed to predict debris hazard arising from the backblast of small rockets. The model is in three parts: Gas dynamics give upper bounds on maximum velocities of jet entrained particles. Aerodynamics give an expression for subsequent motion of debris through still air. A semiempirical study gives an expression describing skin penetration by debris. Computer codes are given for implementation of model.

LEVEL II

(2)

DEVELOPMENT OF A METHOD FOR PREDICTING TRAJECTORIES AND TERMINAL VELOCITIES OF BACKBLAST DEBRIS FROM SMALL ROCKETS

FINAL REPORT

Rush E. Elkins

Dennis R. Keefer

December 1980

Prepared for

U.S. ARMY RESEARCH OFFICE

Under Contract

DAAG29-79-C-0127

University of Tennessee Space Institute

Tullahoma, Tennessee

APPROVED FOR PUBLIC RELEASE

DISTRIBUTION UNLIMITED

TABLE OF CONTENTS

FIGURE LIST

TABLES

SECTION 1

INTRODUCTION

Entrained debris constitutes a widely recognized hazard associated with the firing of rockets and recoilless rifles. Igniter wires, nozzle plugs, propellent chunks, ground debris, or anything else in the path of escaping propellent gases can be entrained and accelerated to speeds sufficient to injure personel or equipment. Characterization of this debris hazard may thus be an important facet in the design of effective weapons.

Section 2 of this paper presents a model for determining a region of hazard in the vicinity of small rockets and tube launched weapons. The model is developed in three parts. The first considers motion of debris in a flow field generated by expanding propellent gases. The second considers motion of debris through ambient air. The third considers impact of the debris with personnel or equipment. These three parts are then combined to give relations for estimating the extent of the debris hazard area.

Section 3 discusses use of the model and analyzes the Viper light antitank rocket, described in Appendix C, as an illustrative example. This section can be used independently of Section 2. The model is

presented in this section both in the form of tabulated equations and in the form of dimensionless plots. Parametric sensitivity of the model is also discussed here; debris drag coefficient is identified as a critical parameter. Appendix D gives computer and calculator codes for implementing this model.

Section 4 discusses shortcomings of the model. While the debris hazard area is estimated with "worst case" considerations, there are circumstances in which particles can be projected outside it with dangerous velocities. Those circumstances can arise when particle shape, plume characteristics, or backblast area give rise to anomolous particle deflections.

SECTION 2

MODEL DEVELOPMENT

This section develops the basic debris hazard model for small rocket backblast. The equation of motion for a particle in a flow is discussed and shown to be too complex for exact implimentation. Several simplifying assumptions are then made which lead to upper bounds on minimum safe standoff distance and maximum dispersion angle. Ideas from fluid mechanics, gas dynamics, and a semiempirical skin penetration criterion are incorporated into the debris hazard model. An effort has been made to express the model in terms of readily attainable parameters and to keep the number of those parameters at a reasonable minimum.

A particle entrained in a gas flow is acted on by aerodynamic forces and by body forces. Equating those forces to the rate of momentum change of the particle leads to an equation of motion for the particle. The aerodynamic forces are conventionally resolved into lift and drag forces which are, respectively, normal and antiparallel to the particle's motion relative to the gas. Gravity is the only body force of significance to the debris hazard problem.

For the present, we will ignore lift and gravity. The effects of those forces will be discussed in Section 4. Even so, a particle's equation of motion is complex:

$$m \frac{d\bar{v}_p}{dt} = \tfrac{1}{2} C_d A \rho |\bar{v}_g - \bar{v}_p| (\bar{v}_g - \bar{v}_p) \qquad (2.1)$$

where m is particle mass, $\bar{v}_p(t)$ is particle vector velocity as a function of time, C_d is particle drag coefficient, ρ is gas density, A is particle velocity-wise projected area, and $\bar{v}_g$ is gas vector velocity. In general, C_d will be a function of velocity, gas temperature, and particle dynamics while A will be a function of particle orientation. In addition, ρ and $\bar{v}_g$ will have time varying spatial distributions due to time variation in the gas source, to turbulent mixing with ambient air, and to dynamic coupling with the particle motion.

The problem in this form is intractable. Nevertheless, it is possible to develop equation (2.1) to arrive at an estimate for maximum particle velocity and maximum particle dispersion. Such considerations will suffice for definition of an area of debris hazard.

Four assumptions will greatly simplify analysis while retaining the essential features of the debris hazard problem. First, a particle will reach a higher velocity in a fully developed plume than in a partially developed one. Second, a particle's motion is not affected by a passing shock. Third, the gas flow field is decoupled from the particle motion. Fourth, rocket motor motion does not affect the debris hazard problem.

The first assumption is suggested by observations of developing supersonic plumes (see Appendix A on supersonic jets). Photographs indicate that, at any given time, a

developing plume can be represented as a truncated version of a fully developed plume (see, for example, Schmidt, 1974). It follows that for whatever velocity a particle reaches in a partially developed plume, there will be further acceleration in the fully developed plume. Since maximum streamline turning angles occur at the nozzle lip, the angular dispersion of particles should be about the same at any time during plume development.

The second assumption is suggested by the fact that a particle's interaction time with shock waves emanating from a small rocket is very short. Observations of the motions of ping pong balls in shock tubes (de Krasinsky, 1975) support this assumption.

The third assumption will be valid when the debris occupies an insignificant fraction of the plume volume. This condition may be violated in the vicinity of the nozzle, where debris loading of the jet can be high. The effect is one of reducing jet momentum and deflecting gas stream lines. In any case, the effect is expected to be a small one since any alteration of flow field occurs only in the nozzle vicinity.

The fourth assumption will be valid so long as gas speeds in the jet are much greater than the speed of the motor. This condition will probably be met in nearly all cases -- typically, a small rocket starts from rest and has a terminal speed less than twenty percent of the gas speed.

With these assumptions, one can set an upper limit on particle velocity by following the motions of single

particles in steady supersonic jets. It is convenient to transform equation (2.1) from a Lagrangian to an Eulerian representation via the chain rule:

$$m\bar{v}_p \cdot \nabla \bar{v}_p = \tfrac{1}{2} C_d A \, \rho |\bar{v}_g - \bar{v}_p| (\bar{v}_g - \bar{v}_p) \tag{2.2}$$

Particle velocity $\bar{v}_p$ has been transformed to spatial coordinates through the relation

$$t = t(\bar{x}) \tag{2.3}$$

which is the time t that the particle occupies position $\bar{x}$.

Given a jet flow field, equation (2.1) can be used in conjunction with a skin penetration model (Lewis, 1978) to predict a region of debris hazard. For each class of debris, one integrates equation (2.2) to the point where $|\bar{v}_p|$ drops below the minimum penetration velocity predicted by the penetration model. The locus of all such points defines the boundary of the debris hazard area.

Although the above procedure might be useful as a check on more approximate procedures, it is not a good choice for a debris hazard model. As will be shown, the minimum safe standoff distance is very sensitive to uncertainties in particle drag coefficients and other parameters. The computational effort required in finding the flow field and then integrating equation (2.2) is not justified by the uncertainty of the results. Results of simpler models are apt to be just as valid.

The model developed in the following paragraphs follows a particle through three phases of its motion. The first phase concerns particle acceleration in the rocket jet. Expressions will be developed for estimating the particle's maximum velocity and maximum angular deviation. The second phase concerns the particle's velocity decay in still air. The third phase concerns the particle's impact with a target. These phases are shown schematically in figure (2.1).

Consider a particle of mass m acted on by a force $\bar{F}(x)$ over a path between two points x_1 and x_2. The speed $v(x)$ of the particle is changed only by the component of $\bar{F}$ which is directed along the path. That component will be designated $\bar{F}_s$. The particle's change of speed Δv between points x_1 and x_2 is then given by

$$\Delta v = \left[\frac{2}{m} \int_{x_o}^{x_1} \bar{F}_s(x) \cdot \overline{ds} \right]^{\frac{1}{2}} \tag{2.4}$$

where integration is pathwise and $\overline{ds}$ is an element of the particle's path $S(x)$ between x_o and x_1. (This is equivalent to integrating the left side of equation (2.2)). An upper limit can be written for Δv:

$$\Delta v \leq \left[\frac{2L}{m} |F_s|_{max} \right]^{\frac{1}{2}} \tag{2.5}$$

where L is the length of S and $|F_s|_{max}$ is the maximum magnitude of F_s.

For a given path, $\bar{F}_s$ is equal to the pathwise component of the right hand side of equation (2.2).

$$\bar{F}_s = \tfrac{1}{2} C_d A_d \rho |\bar{v}_g - \bar{v}_p| (\bar{v}_g - \bar{v}_p)_s \tag{2.6}$$

where $(\bar{v}_g - \bar{v}_p)_s$ is the pathwise component of $(\bar{v}_g - \bar{v}_p)$. Equation (2.5) will continue to be satisfied if an upper bound on $|F_s|$ is substituted for $|F_s|_{max}$. From vector analysis, we have

$$|\bar{v}_g - \bar{v}_p| |(\bar{v}_g - \bar{v}_p)_s| \leq (\bar{v}_g - \bar{v}_p) \cdot (\bar{v}_g - \bar{v}_p) \tag{2.7}$$

Substitution of (2.6) and (2.7) into (2.5) leads to

$$\Delta v \leq \left[\frac{L}{M} C_d A \rho (\bar{v}_g - \bar{v}_p) \cdot (\bar{v}_g - \bar{v}_p) \right]_{max}^{\frac{1}{2}} \tag{2.8}$$

This relationship states that the speed change of a particle is less than it would have been had the particle been acted on by a constant force equal to the global maximum.

Relationship (2.8) is much simplified when $\bar{v}_p$ is assumed to be negligible. There is good justification to do this. In a small rocket, particles small and light enough to follow the gas flow closely will have short ranges once ejected from the plume. The larger particles, owing to their larger masses, will respond more sluggishly to the aerodynamic forces of the jet so that $|\bar{v}_p| << |\bar{v}_g|$ becomes the expected

condition. In any event, the effect of assuming $\bar{v}_p = 0$ is generally to overestimate Δv in equation (2.4), so that relationship (2.8) remains valid. With these considerations, relationship (2.8) can be written

$$\Delta v \leq \left(\frac{L}{m} C_d A \ \rho v_g^2\right)_{max}^{\frac{1}{2}} \tag{2.9}$$

where

$$v_g^2 = \bar{v}_g \cdot \bar{v}_g \tag{2.10}$$

As previously noted, C_d and A can be complicated functions of particle dynamics and aerodynamics. We will here suppose that constant values can be chosen for each such that the inequality in (2.9) is not violated. How those values might be chosen is deferred to later discussion. Relationship (2.9) becomes

$$\Delta v \leq \left(\frac{L \ C_d A}{m}\right)^{\frac{1}{2}} \left(\rho \ v_g^2\right)_{max}^{\frac{1}{2}} \tag{2.11}$$

The quantity ρv_g^2 in relation (2.11) is the local momentum flux density of the plume. If the gas in the plume undergoes an isentropic expansion, then ρv_g^2 has a maximum determined by the gas dynamics. (The assumption of an isentropic expansion may not be valid if a significant amount of heat is added during the expansion. This may occur in a small rocket if significant amounts of fuel are burned outside the combustion chamber.)

In an isentropic expansion (Van Wylen, p.358),

$$v_g^2 = \frac{2kRT_o}{k-1}\left(1 - \frac{T}{T_o}\right) \tag{2.12}$$

$$\rho = \rho_o \left(\frac{T}{T_o}\right)^{\frac{1}{k-1}} \tag{2.13}$$

$$\frac{T}{T_o} = \left(\frac{P}{P_o}\right)^{\frac{k-1}{k}} \tag{2.14}$$

where the subscript o denotes stagnation conditions and where k is ratio of specific heats, R is gas constant, T is temperature, and P is pressure. Substituting (2.14) into (2.12) and (2.13) and noting that

$$RT_o\rho_o = P_o \, , \tag{2.15}$$

one is lead to

$$\rho v^2 = \frac{2kP_o}{k-1}\left(\left(\frac{P}{P_o}\right)^{1/k} - \frac{P}{P_o}\right) \tag{2.16}$$

Equation (2.16 is plotted in figure (2.2) for k equal to 1.4, corresponding to air, and for k equal to 1.16, corresponding to hot combustion gases. The figure shows variation in the dimensionless drag force, $\frac{\rho v^2}{2P_o}$, as the flow expands from stagnation $\left(\frac{P}{P_o} = 1\right)$ to vacuum $\left(\frac{P}{P_o} = 0\right)$. Note that the peak values of these curves differ little in magnitude and occur at approximately the same values of pressure ratio. This suggests that a particle drag model depending on maximum momentum flux density should be insensitive to uncertainties in k.

The rapid fall off in dimensionless drag force as $\frac{P}{P_o}$ approaches zero is an important consideration in laser doppler velocimetery. That technique assumes that drag forces are large enough that entrained particles follow the flow streamlines everywhere. In an underexpanded supersonic jet, where $\frac{P}{P_o}$ can easily be as small as 0.001, particles may not follow the flow.

Differentiating equation (2.16) with respect to $\frac{P}{P_o}$ and setting the result equal to zero leads to

$$\frac{P}{P_o} = (k)^{\frac{k}{1-k}} \tag{2.17}$$

for the pressure ratio corresponding the maximum momentum flux density. Substitution of (2.17) into (2.16) leads to

$$\rho v^2 = 2P_o k^{\frac{1}{1-k}} \tag{2.18}$$

for the maximum momentum flux density. Equation (2.18) states that the maximum momentum flux, and hence the maximum drag force on a particle, is directly proportional to the stagnation pressure and weakly dependent on the ratio of specific heats over its normal range. One can use equation (2.14) and the expression for Mach number M,

$$M^2 = \frac{2}{k-1}\left(\frac{T_o}{T} - 1\right) \tag{2.19}$$

to show that the maximum in momentum flux density occurs in an isentropic expansion at a Mach number equal to $\sqrt{2}$. This is very early in the expansion and will probably occur within the nozzle.

Substituting (2.18) into (2.11) leads to

$$\Delta v \leq \left(\frac{2LC_d A\ P_o}{m} k^{\frac{1}{1-k}}\right)^{\frac{1}{2}} \tag{2.20}$$

for an upper bound on the velocity change of a particle entrained in an isentropic expansion over a length L.

The value of L will depend on the jet's geometry. We propose, tentatively, that it be set equal to the length λ of the bottle shock, noting that, downstream of the Mach disc, the momentum flux density is rapidly dispersed by turbulent mixing (Che-Haing, 1969). This choice is further motivated by the fact that the jet will scale on λ (Che-Haing, 1969), so that setting $L=\lambda$ is in error by at worst a multiplicative constant. It will be shown later that safe standoff distance is not critically dependent on L.

Lewis (1966) gives an empirical expression for the wavelength λ as a function of exit Mach number M_E and of the ratio of exit pressure P_E to ambient pressure P_A:

$$\frac{L}{d_E} = 0.69 M_E \left(\frac{k P_E}{P_A} \right)^{\frac{1}{2}} \tag{2.21}$$

where d_E is the nozzle exit diameter. This equation has been verified over a wide range of values for M_E and $\frac{P_E}{P_A}$. It might be noted that Love (1959) gives an expression which differs considerably from equation (2.21). Lewis comments that, between investigators, there is frequently much scatter in these data.

The exit Mach number can be found from

$$\frac{A_E}{A^*} = \frac{1}{M_E} \left[\left(\frac{2}{k+1} \right) \left(1 + \frac{k-1}{2} M_E^2 \right) \right]^{(k+1)/2(k-1)} \tag{2.22}$$

where A_E is the nozzle exit area and A^* is the throat area. The exit pressure ratio can be expressed as (Van Wylen, 1963)

$$\frac{P_E}{P_A} = \frac{P_o}{P_A} \left[1 + \frac{(k-1)}{2} M_E^2 \right]^{k/(1-k)} \tag{2.23}$$

Once clear of the bottle shock region (see Appendix A on jet structure), a particle interacts with a decaying jet plume where gas momentum flux density drops rapidly with increasing distance from the source. Those particles of most interest to the debris hazard problem are unlikely to be further accelerated in this region of rapidly dwindling jet influence. Within a distance of a few λ, the more dangerous particles will be traveling much faster

than the surrounding gases. There, setting $\bar{v}_g = 0$ in equation (2.2) becomes a valid approximation. (Note that if the particles are accelerated to supersonic speeds, they can outrun the shock wave generated by the starting jet. Setting $\bar{v}_g = 0$ in that case is not an approximation, but a statement of the observed physics. Schmidt (1974) has taken remarkable photographs of such particles occurring in the muzzle blast of an M-16 rifle.)

From equation (2.2), the motion of a particle through still air with no body forces is

$$m\,v\,\frac{dv}{dx} = -\tfrac{1}{2}C_d A \rho_A v^2 \tag{2.24}$$

where ρ_A is the air density and where x has been taken to be in the direction of particle motion. For m, C_d, A and ρ_A constant, equation (2.24) integrates to

$$x = \frac{m}{C_d A\,\rho_A} \ln\left[\frac{v_o}{v}\right] \tag{2.25}$$

where v_o is the initial velocity. Equation (2.25) expresses the distance required for a particle to drop in speed from v_o to v.

Lewis (1978) has shown that a particle's probability of penetration is a monotonically increasing function of $\frac{mv^2}{QA_p}$ where m is the particle's mass, v is its velocity, A is its area, and Q is a parameter describing the target's material properties (see Appendix B). It follows that if the probability of penetration is not to exceed some given level, then $\frac{mv^2}{QA}$ must not exceed some number n:

$$\frac{mv^2}{QA} < n \tag{2.26}$$

or $$v < \left(\frac{Q_p A}{m}\right)^{\frac{1}{2}} \tag{2.27}$$

where

$$Q_p = nQ \tag{2.28}$$

will be termed the penetration parameter.

Equations (2.20), (2.25), and (2.27) can now be combined to form the basic model for calculating safe standoff distance from a small rocket. A safety criterion can be set by demanding that a particle, accelerated to the maximum speed given by equation (2.20), must be slowed via drag, described in equation (2.25), below the minimum penetration speed given in equation (2.27). This leads to

$$S > \frac{m}{2C_d A \rho_A}\left[\ln \frac{2LC_d P_o}{Q_p} + \frac{1}{k-1} \ln k\right] + L \tag{2.29}$$

or, in dimensionless expression

$$\frac{A\rho_A S}{m} > \frac{1}{2C_d}\left[\ln \frac{2LC_d P_o}{Q_p} + \frac{1}{k-1} \ln k\right] + \frac{2C_d A L}{m} \tag{2.30}$$

where S is the standoff distance.

The angular dispersion of the debris could be calculated by integrating equation (2.2) over a large number of cases. As with standoff distance, however, uncertainties in the problem lead

us to search for a simplified means of establishing an upper bounds on dispersion angle. Gas dynamics is helpful here.

The largest angle through which a gas molecule can turn in a supersonic expansion is given by the Prandtl-Meyer turning angle (Shapiro, 1953). Thus, in the plume of an underexpanded rocket, no streamline will have an inclination to the axis larger than the sum of the nozzle divergence and the Prandtl-Meyer turning angle for conditions at the nozzle lip. See figure (2.3). In the absence of lift and body forces, an entrained particle moves away from the axis at no angle larger than that of the most inclined streamline. We will take this as the upper bounds on particle dispersion. Conditions under which that "upper bounds" might be exceeded will be discussed in a later section.

The turning angle θ for a Prandtl-Meyer expansion is given by Shapiro (1953):

$$\theta = -\operatorname{atan}\,(M^2-1)^{\frac{1}{2}} + \left(\frac{k+1}{k-1}\right)^{\frac{1}{2}} \operatorname{atan}\left(\frac{k-1}{k+1}\,(M^2-1)\right)^{\frac{1}{2}} \tag{2.31}$$

This represents the angle through which a flow turns in expanding from Mach number unity to Mach number M.

To calculate the maximum angular streamline deviation θ_{max} for an underexpanded jet, the following procedure can be followed. First, determine a k appropriate for the propellent gases. Next determine an ambient turning angle θ_A by substituting M_A into equation (2.31), where

$$M_A = \left(\frac{2}{k-1}\right)^{\frac{1}{2}} \left(\left(\frac{P_c}{P_A}\right)^{\frac{k-1}{k}} - 1\right)^{\frac{1}{2}} \tag{2.32}$$

is the Mach number of a flow expanded from chamber pressure P_o to ambient pressure P_A. Then determine a nozzle exit turning angle θ_E by substituting M_E into equation (2.31), where M_E is the Mach number at the nozzle exit plane, satisfying

$$\frac{A_E}{A^*} = \frac{1}{M_E}\left[\left(\frac{2}{k+1}\right)\left(1 + \frac{k-1}{2} M_E^2\right)\right]^{(k+1)/2(k-1)} \tag{2.33}$$

with A_E being the exit area and A^* the throat area of the nozzle. If θ_N is the nozzle divergence angle, then the maximum streamline deviation is

$$\theta_{max} = \theta_A - \theta_E + \theta_N \tag{2.34}$$

Tube launched rockets require some special considerations. A system in which the rocket nozzle's exit plane is placed at or near the launch tube's breech will have essentially the same debris hazard as the rocket alone. When the rocket is placed higher up in the launch tube, the launch tube can be expected to act as an extension of the rocket nozzle. Nozzle exit plane configuration for the debris hazard model is then the launch tube breech configuration. Usually, this will not much change the standoff distance and will narrow the dispersion angle. When the rocket is placed several diameters up the launch tube, the dispersion may widen.

This completes the basic debris hazard model. Equation (2.29), for minimum safe standoff distance, and equation (2.34), for maximum dispersion, together define a sector of a circle to the rear of a rocket where a debris hazard may exist. There are two

semiempirical parameters in the model: Q_p, describing the target material, and L, describing the particle acceleration distance. Model usage is described in Section 3.

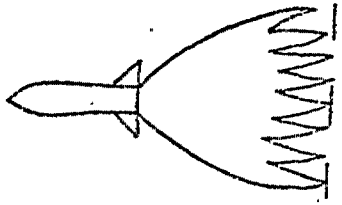

Phase 1
Debris interacts
with jet. Equation (2.11)

Phase 2
Debris interacts with
still air. Equation (2.25)

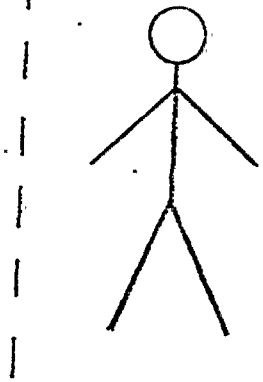

Phase 3
Debris impacts
target. Equation (2.27)

Figure (2.1) - Illustration of three phases of the basic debris hazard model.

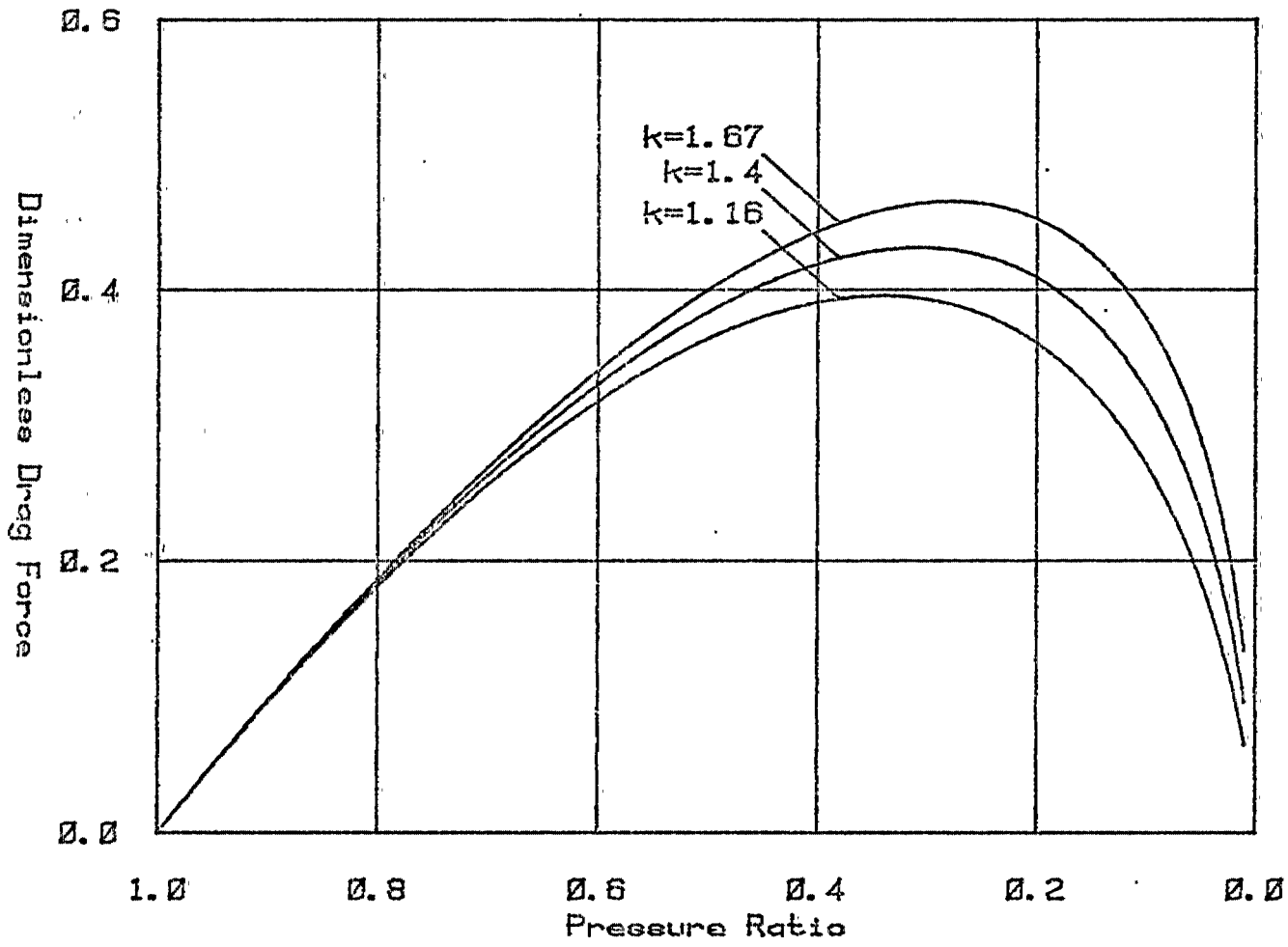

Figure 2.2 - Plot of Dimensionless Drag Force $\left(\frac{\rho v^2}{2P_o}\right)$ versus Pressure Ratio $\left(\frac{P}{P_o}\right)$.

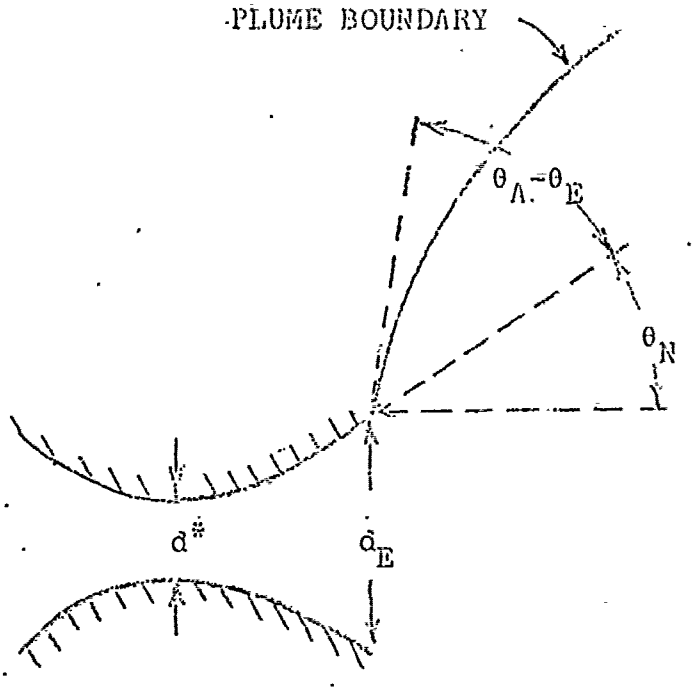

Figure 2.3 - Defining diagram for nozzle geometry and initial plume turning angle.

SECTION 3

MODEL USAGE

This section illustrates use of the debris hazard model developed in Section 2. The Viper, a shoulder launched antitank rocket, is used to aid in the illustration. A step by step procedure is presented for determining standoff distance and dispersion angle from the pertinent physical data. Interactive computer codes incorporating that procedure are given in Appendix D. Finally, a series of dimensionless plots are shown which identify critical parameters in the model.

The debris hazard model of this report requires knowledge of eleven parameters -- five to describe the rocket motor, three to describe the debris, one to describe the target, and two to describe the ambient air. Viper characteristics are summarized in Appendix C, and target toughness is discussed in Appendix B. (Additionally, there is a semiempirical constant which relates debris acceleration length L to jet primary wavelength λ. In the present implementation of the model, L is taken to be equal to λ.) These parameters are listed in Appendix C.

The next few paragraphs show the use of the parameters of Table (C.1) to determine standoff distance and dispersion angle for the Viper. The procedure is outlined in figures(3.1) and (3.2).

The first calculation is the determination of jet primary wavelength λ from equation (2.21). This equation requires the exit Mach number M_E, which can be determined from equation (2.22) (see Appendix E), and the exit plane pressure P_E, which can be determined from equation (2.23). (Equations (2.22) and (2.23) are represented in figures (3.3) and (3.4).) For Viper, $M_E = 2.07$, $P_E = 8.03 \times 10^6$ N/m^2, and $\lambda = 0.85$ m. Substitution of these values and of values from Table (C.1) into equation (2.29) gives a minimum safe standoff distance S = 33m for Viper's detente fingers striking people wearing summer weight uniforms.

Calculation of dispersion angle is as follows. Equation (2.31), using M_E determined in the standoff calculation, gives $\theta_E = 35^o$. Equations (2.32) and (2.31) give $M_A = 4.27$ and $\theta_A = 102^o$. (Equations (2.32) and (2.31) are represented in figures (3.5) and (3.6).) Substitution of θ_E, θ_A and θ_N (from Table C.1) into equation (2.34) gives $\theta_{max} = 78^o$.

In summary, the model predicts that a hazardous region exists behind the rocket to a distance of 33 meters from the nozzle and to 78 degrees off axis. In a complete analysis, the standoff distance would be calculated for each type of debris. The procedures outlined above have been incorporated into the computer codes documented in Appendix D.

In one of Viper's proposed configurations, the launch tube is extended rearward several centimeters beyond the rocket nozzle exit plane. In that case, it is appropriate to regard the launch tube as an extension of the nozzle. The nozzle exit diameter d_E should then be set to the launch tube inside diameter of 0.0793 m, and the nozzle divergence angle should be set to 0^o. Calculating debris hazard as before, one finds for standoff distance, S = 34 m, and for off axis divergence angle, $\theta_{max} = 52^o$. Thus, a short launch tube extension has little effect on standoff distance, but reduces the dispersion angle.

It might be noted that, in the above example, S is much greater than L. This will generally be the case if there are particles accelerated to speeds well in excess of that necessary to cause damage. The error introduced by dropping the last term in equations (2.29) and (2.30) is, therefore, apt to be small. With these considerations, one can neglect that term and express minimum standoff distance by rewriting equation (2.30):

$$\frac{A_p \rho S}{m} = \frac{1}{2C_d} \left(\ln C_d + \ln \frac{LP_o}{Q_p} + \frac{1}{1-k} \ln k \right) \qquad (3.1)$$

Equation (3.1) is plotted in figures (3.7) and (3.8) for several drag coefficients and for specific heat ratios of 1.16 and 1.67. The variation of equation (3.1) with k over the range $1.15<k<1.67$ is slight--see figure (3.7). Note,

however, that there is an implicit variation with k contained in L.

Figure (3.7) covers a parameter range likely for small rockets and unarmored personnel. Two points are noteworthy here. First, the standoff distance is only weakly a function of L for $\frac{LP_o}{Q_p}$ greater than about 20. This means that the estimated standoff distance is not much affected by errors in estimation of L. Such behavior is generally desirable for semiempically determined parameters. Second, the standoff distance is very strongly a function of drag coefficient. Since drag coefficients can vary sharply with particle geometry and dynamics (Sadeh, 1975), this causes a serious and unavoidable uncertainty in the debris hazard model. Specifications of drag coefficients are likely to be the overriding source of undertainty in any debris hazard model. Therefore, further sophistication in the jet fluid dynamic model is likely to be unproductive. The reader is referred to the discussion in Section 4.

Figure (3.8), for small values of $\frac{LP_o}{Q_p}$, covers a range that might be pertinent to armored personnel. The standoff distance for this range varies rapidly with $\frac{LP_o}{Q_p}$ and chaotically with drag coefficient. Clearly, a large margin of safety should be applied for positions in this range.

Figure (3.9) illustrates the quantity $\theta_o = (\theta_A - \theta_E)$ as a function of ambient pressure ratio P_o/P_A, exit to throat nozzle diameter ratio d_E/d^*, and three values of specific heat ratio. The angle θ_o represents the maximum off axis divergence of fluid stream lines for a straight supersonic nozzle. These figures can be used in lieu of evaluating equation (2.31). Evidently, θ_o is a strong function of all three of its arguments, P_o/P_A, d_E/d^*, and k.

Helium, with a mass density near that of typical combustion products, is occasionally used in modeling chemical rocket jets. But, helium has a specific heat ratio of 1.67. The strong dependence of θ_o on k argues that caution be used in deriving quantitative conclusions from such experiments.

Figure (3.1). Outline for Calculation of Standoff Distance.

For standoff distance S, use equation (2.29):

$$S = \frac{m}{2C_d A \rho_A}\left[\ln \frac{2LC_d P_o}{Q_d} + \frac{1}{k-1}\ln k\right] + L$$

A) For m, C_d, A, ρ_A, P_o, and k, see Table (3.1)

B) For skin penetration parameter Q_p, see Appendix B

C) For acceleration length L use equation (2.21)

$$L = \lambda = 0.69\, M_E d_E \left(\frac{kP_E}{P_A}\right)^{1/2}$$

1) For d_E, k and P_A, see Table (3.1)

2) For exit Mach number M_E, use equation (2.22)

$$\left(\frac{d_E}{d^*}\right)^2 = \frac{1}{M_E}\left[\left(\frac{2}{k+1}\right)\left(1 + \frac{k-1}{2} M_E^2\right)\right]^{\frac{(k+1)}{2(k-1)}}$$

a) For d^*, see Table (3.1)

b) See Appendix E for inversion of equation(2.22)

3) For exit plane pressure P_E, use equation (2.23)

$$P_E = P_o\left[1 + \frac{(k-1)}{2} M_E^2\right]^{k/(1-k)}$$

Figure (3.2). Outline for Calculation of Dispersion Angle.

For dispersion half angle θ_{max}, use equation (2.34)

$$\theta_{max} = \theta_A - \theta_E + \theta_N$$

A) For θ_N, see Table (3.1)

B) For θ_E, substitute M_E into equation (2.31)

$$\theta_E = -\text{atan}\left(M_E^2 - 1\right)^{\frac{1}{2}} + \left(\frac{k+1}{k-1}\right)^{\frac{1}{2}} \text{atan}\left(\frac{k-1}{k+1}(M_E^2 - 1)\right)^{\frac{1}{2}}$$

1) For k, see Table (3.1)

2) For exit Mach number M_E, use equation (2.22)

$$\left(\frac{d_E}{d^*}\right)^2 = \frac{1}{M_E}\left[\left(\frac{2}{k+1}\right)\left(1 + \frac{k-1}{2}M_E^2\right)\right]^{k+1/2(k-1)}$$

a) For d_E and d^*, see Table (3.1)

b) See Appendix E for inversion of equation (2.22)

C) For θ_A, substitute M_A into equation (2.31)

$$\theta_A = -\text{atan}\left(M_A^2 - 1\right)^{\frac{1}{2}} + \left(\frac{k+1}{k-1}\right)^{\frac{1}{2}} \text{atan}\left(\frac{k-1}{k+1}\left(M_A^2 - 1\right)\right)^{\frac{1}{2}}$$

1) For M_A, use equation (2.32)

$$M_A = \left(\frac{2}{k-1}\right)^{\frac{1}{2}}\left(\left(\frac{P_o}{P_A}\right)^{(k-1)/k} - 1\right)^{\frac{1}{2}}$$

a) For P_o and P_A, see Table (3.1)

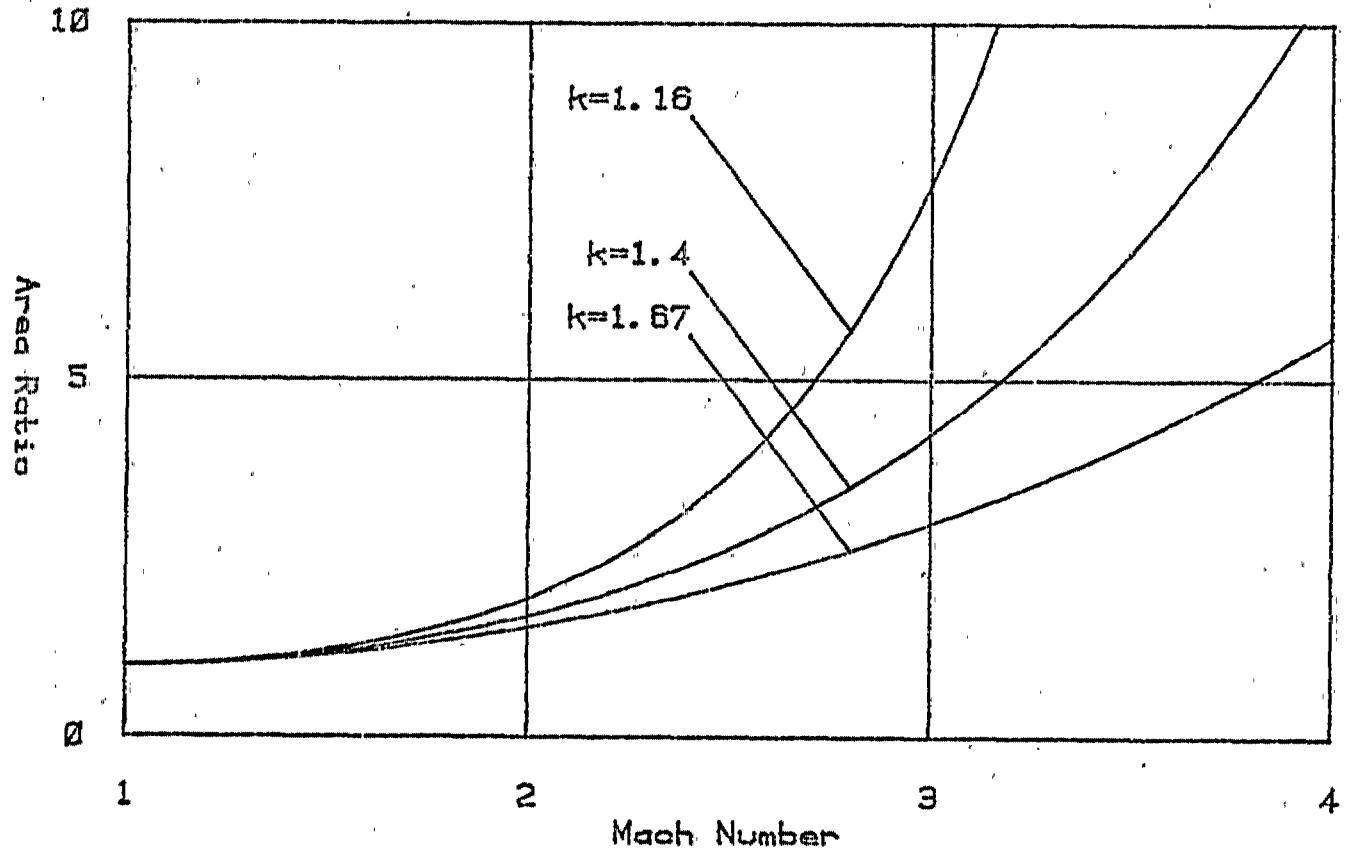

Figure 3.3 - Area Ratio $\left(\frac{A_E}{A^*}\right)$ versus Mach Number (M_E) for an adiabatic expansion.

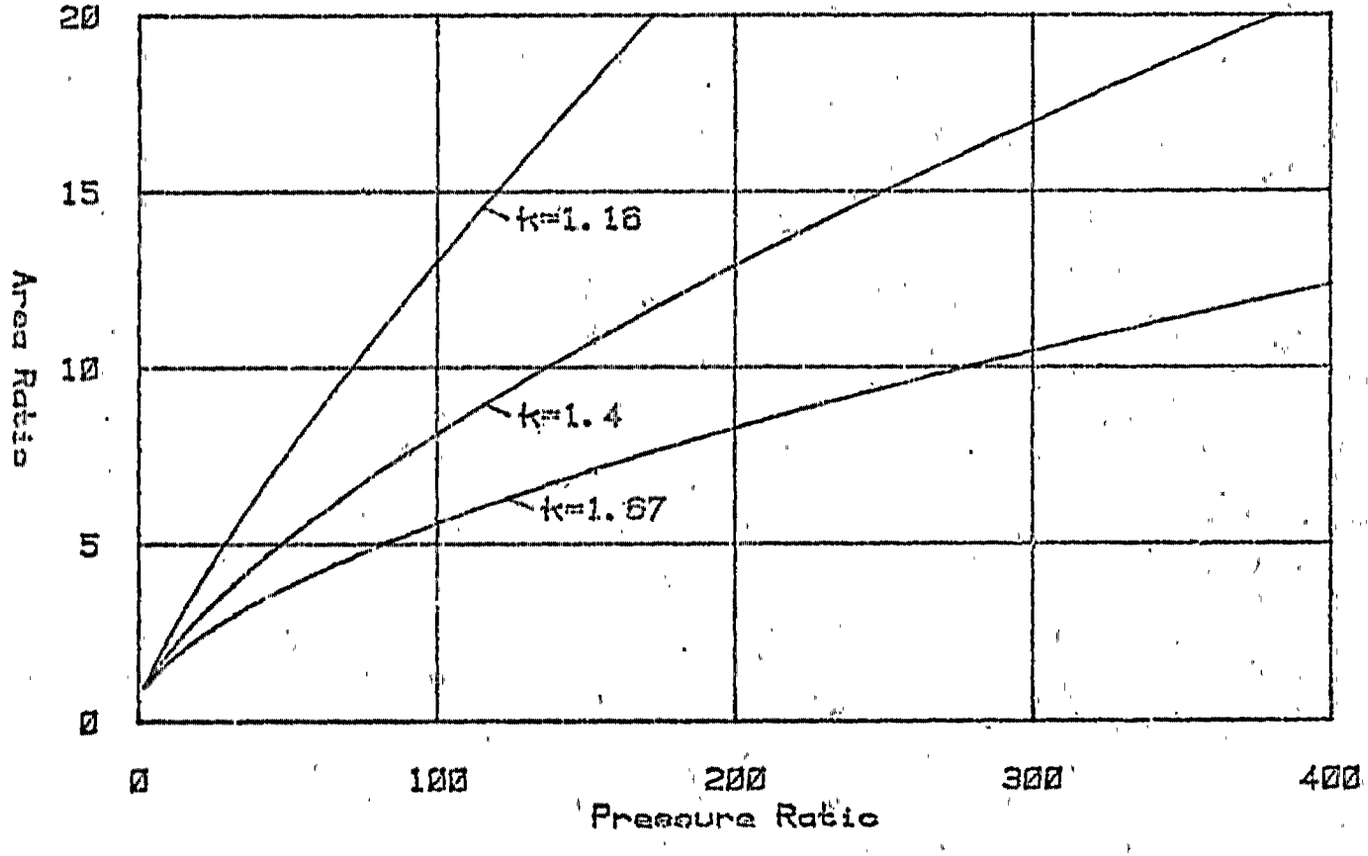

Figure 3.4 – Area Ratio $\left(\frac{A_E}{A^*}\right)$ versus Pressure Ratio $\left(\frac{P_o}{P_E}\right)$ for an adiabatic expansion.

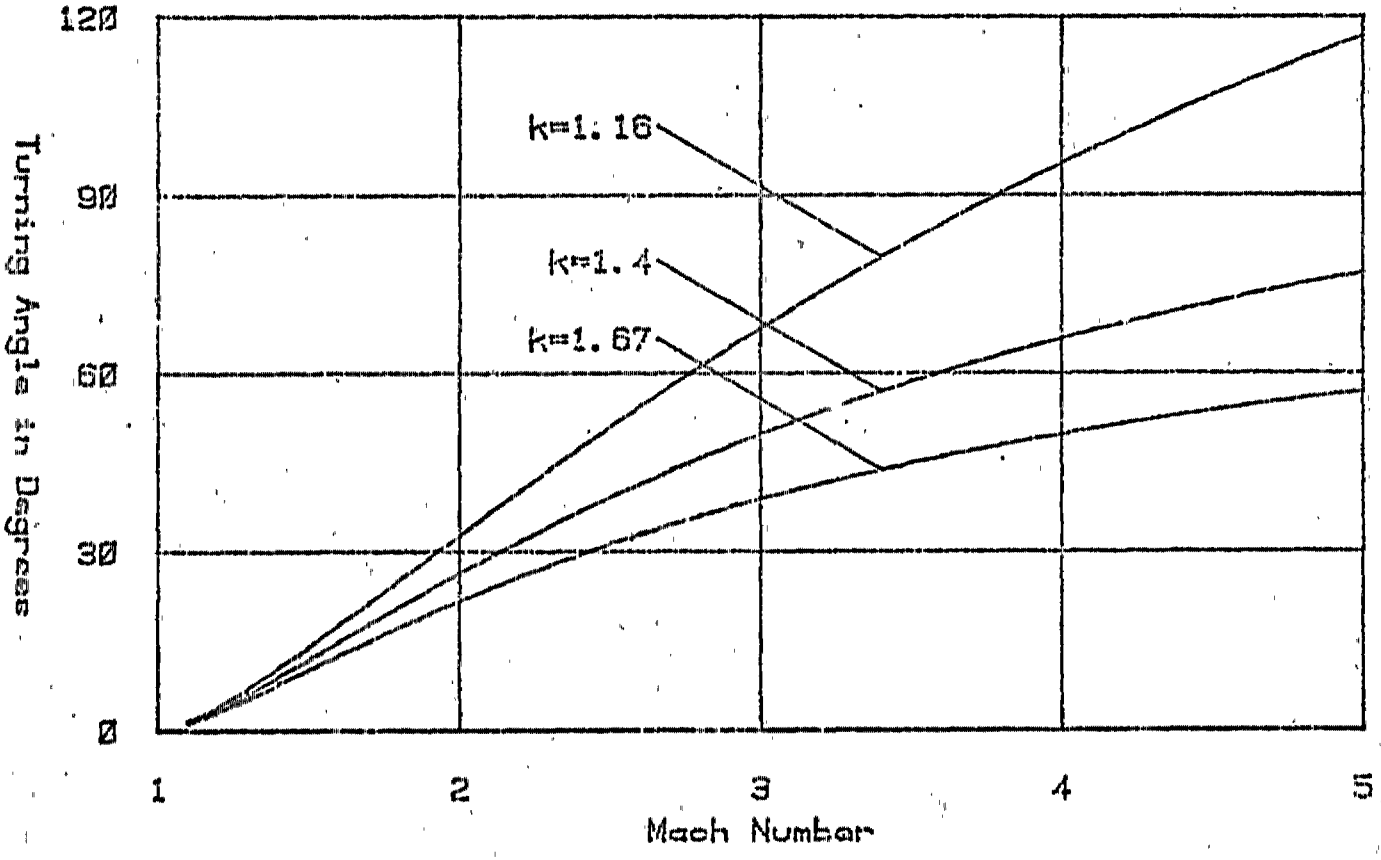

Figure 3.5 - Prandtl-Meyer turning angle versus Mach number, equation (2.31).

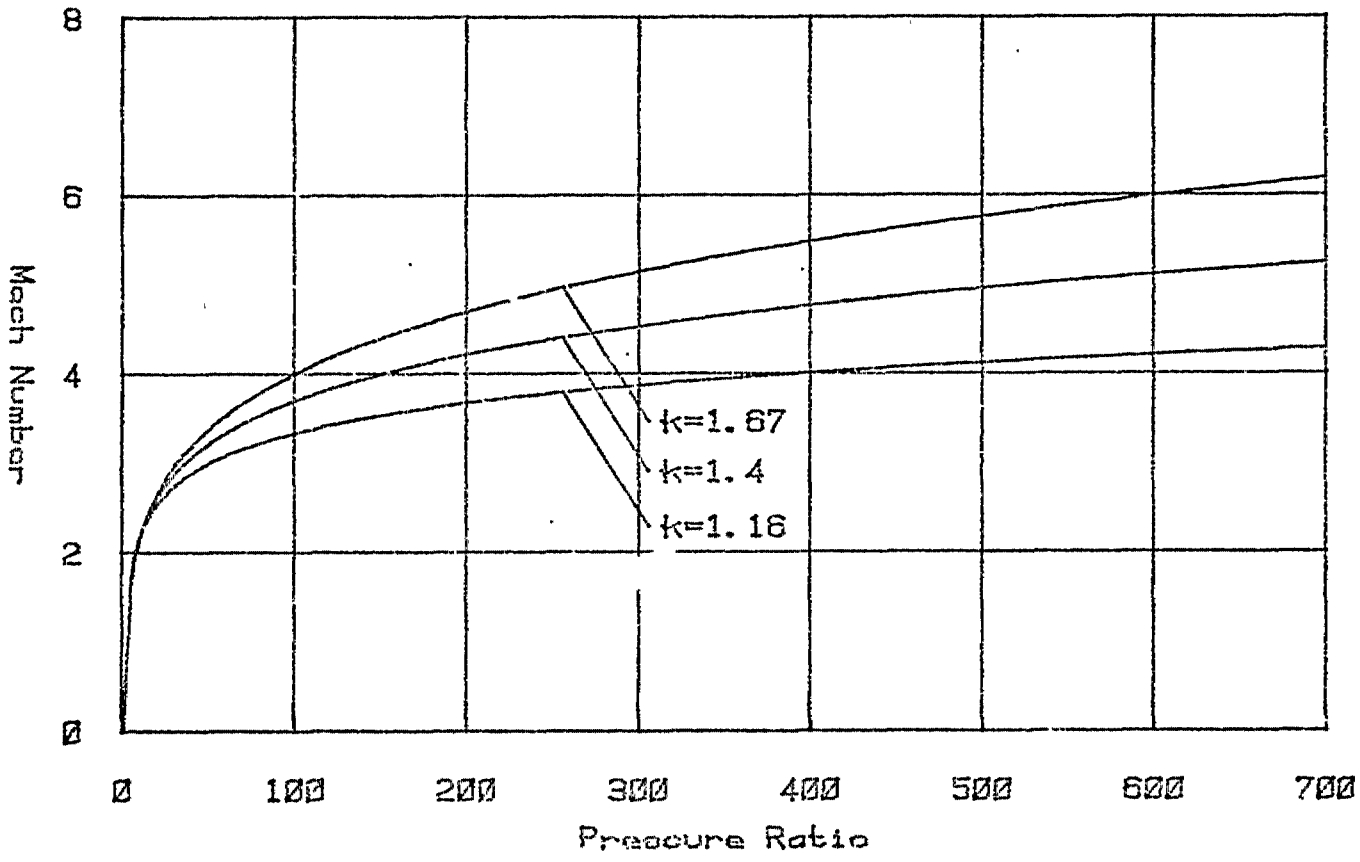

Figure 3.6 - Mach Number vs Pressure Ratio $\left(\frac{P_o}{P}\right)$ for an adiabatic expansion.

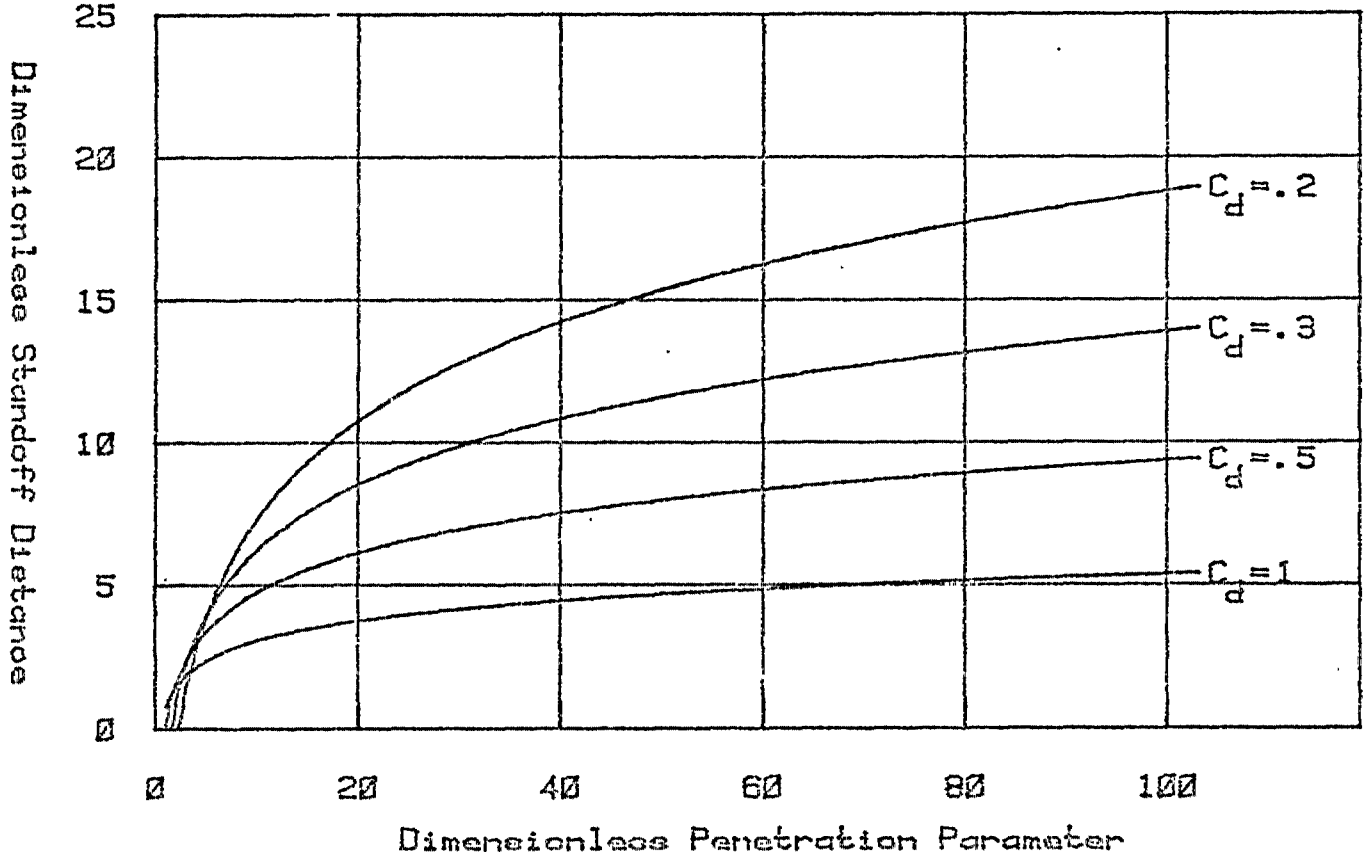

Figure 3.7(b) - Dimensionless Standoff Distance $\left(\frac{A\rho S}{m}\right)$ versus Dimensionless Penetration Parameter $\left(\frac{LC_dP_o}{Q_p}\right)$ for k=1.67.

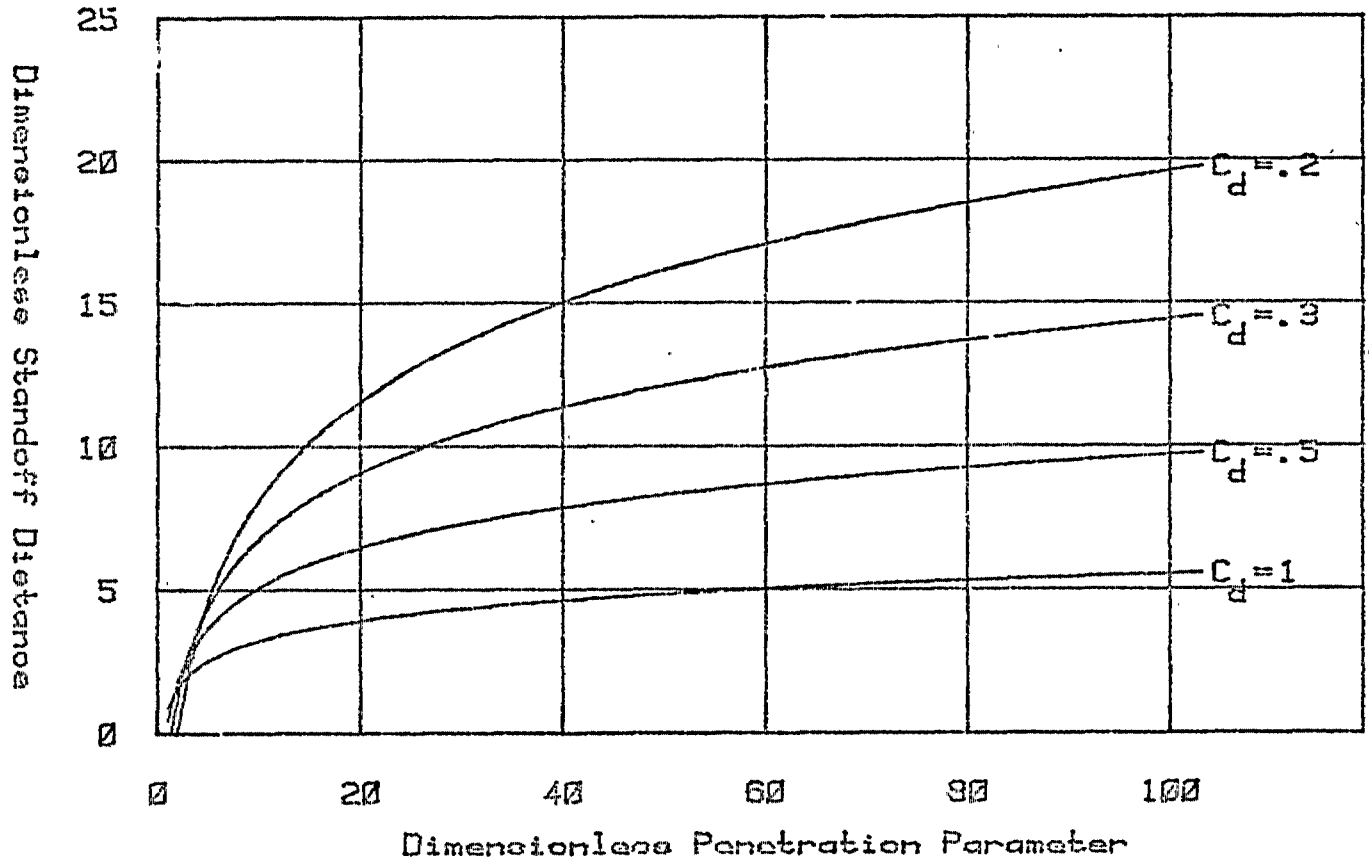

Figure 3.7(a) - Dimensionless Standoff Distance $\left(\frac{A\rho S}{m}\right)$ versus Dimensionless Penetration Parameter $\left(\frac{LC_dP_o}{Q_p}\right)$ for k=1.16.

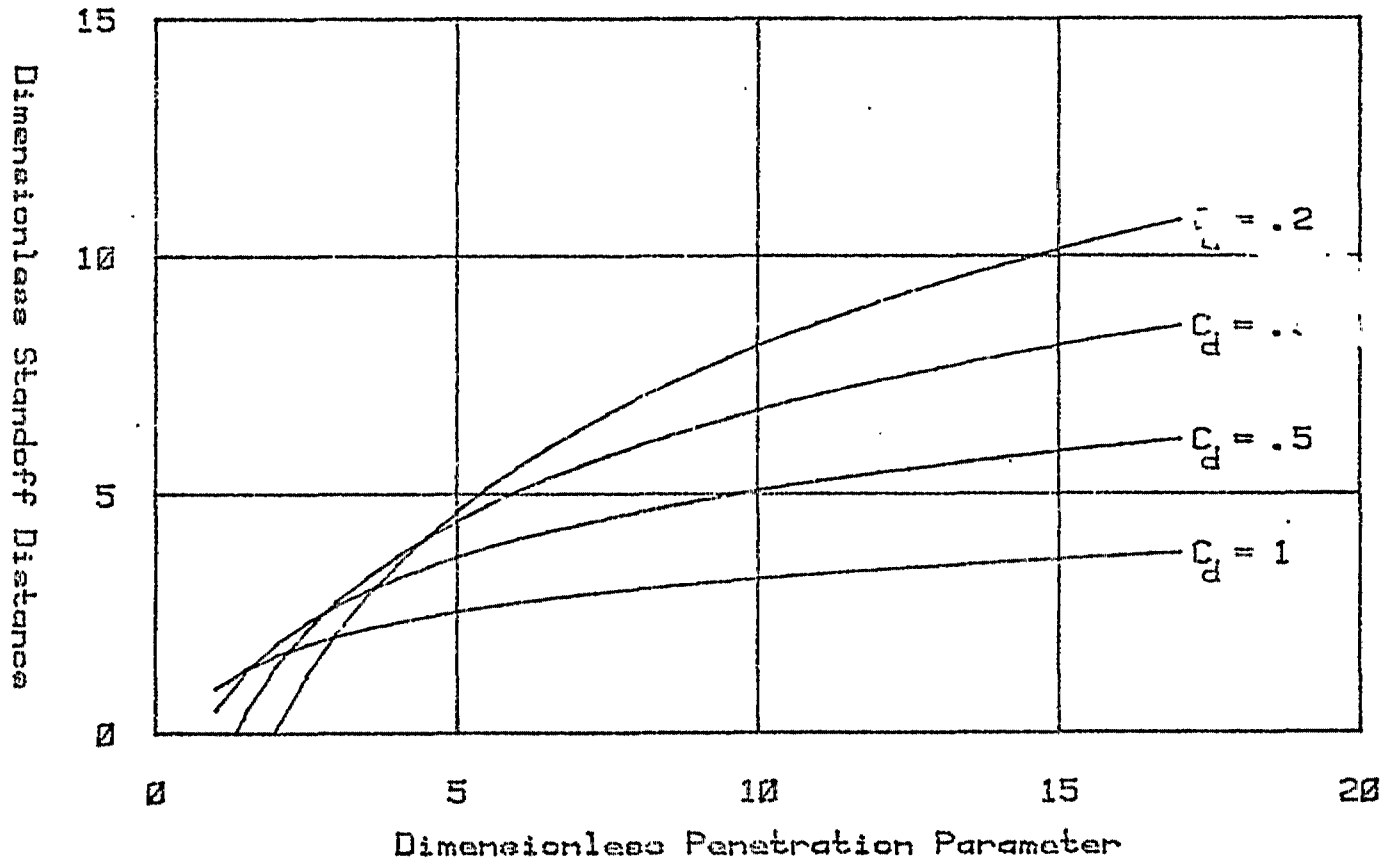

Figure 3.8(a) - Dimensionless Standoff Distance $\left(\frac{A\rho S}{m}\right)$ versus Dimensionless Penetration Parameter $\left(\frac{LC_dP_o}{Q_p}\right)$ for k=1.16.

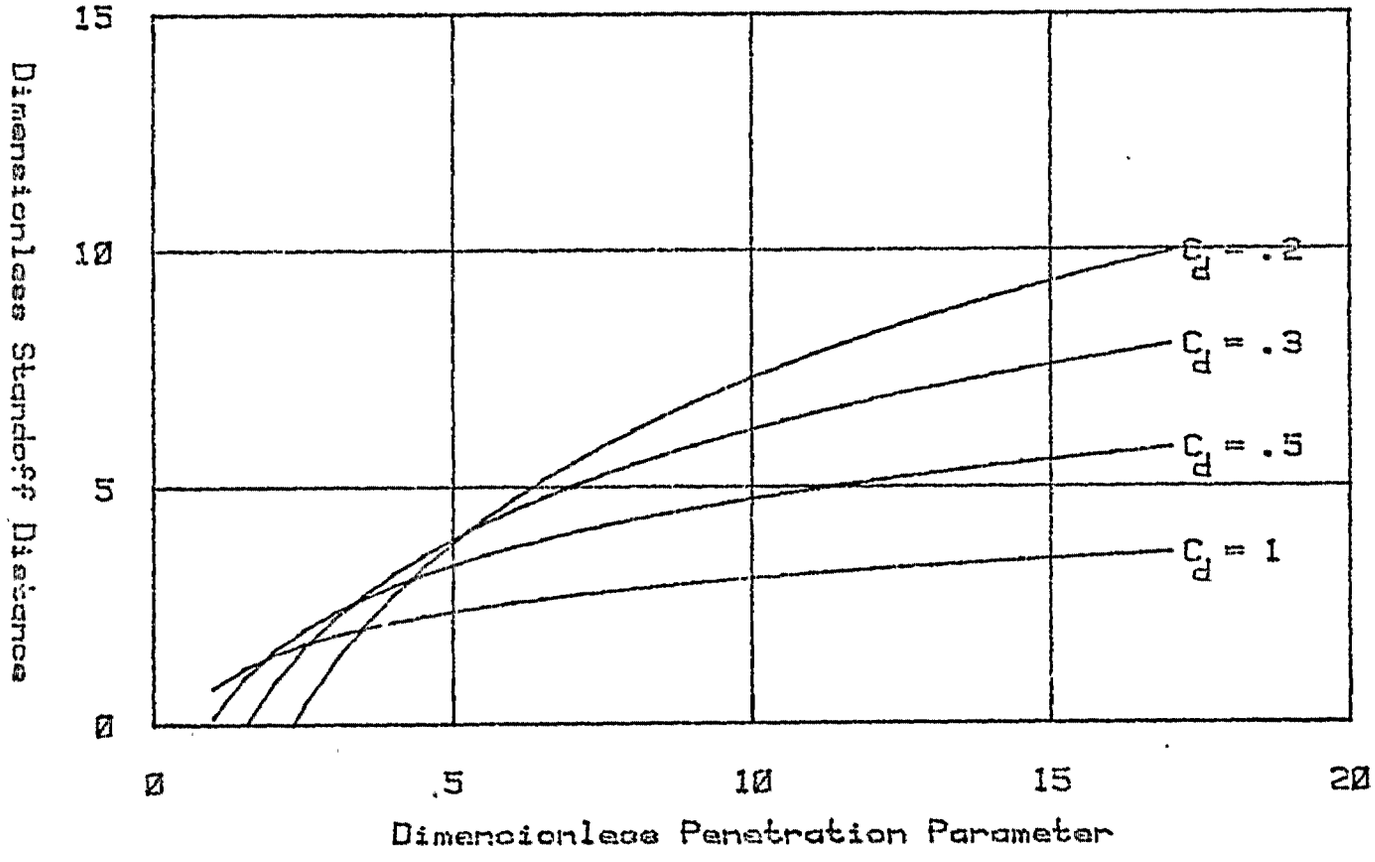

Figure 3.8(b) - Dimensionless Standoff Distance $\left(\frac{A\rho S}{m}\right)$ versus Dimensionless Penetration Parameter $\left(\frac{LC_dP_o}{Q_p}\right)$ for k=1.67.

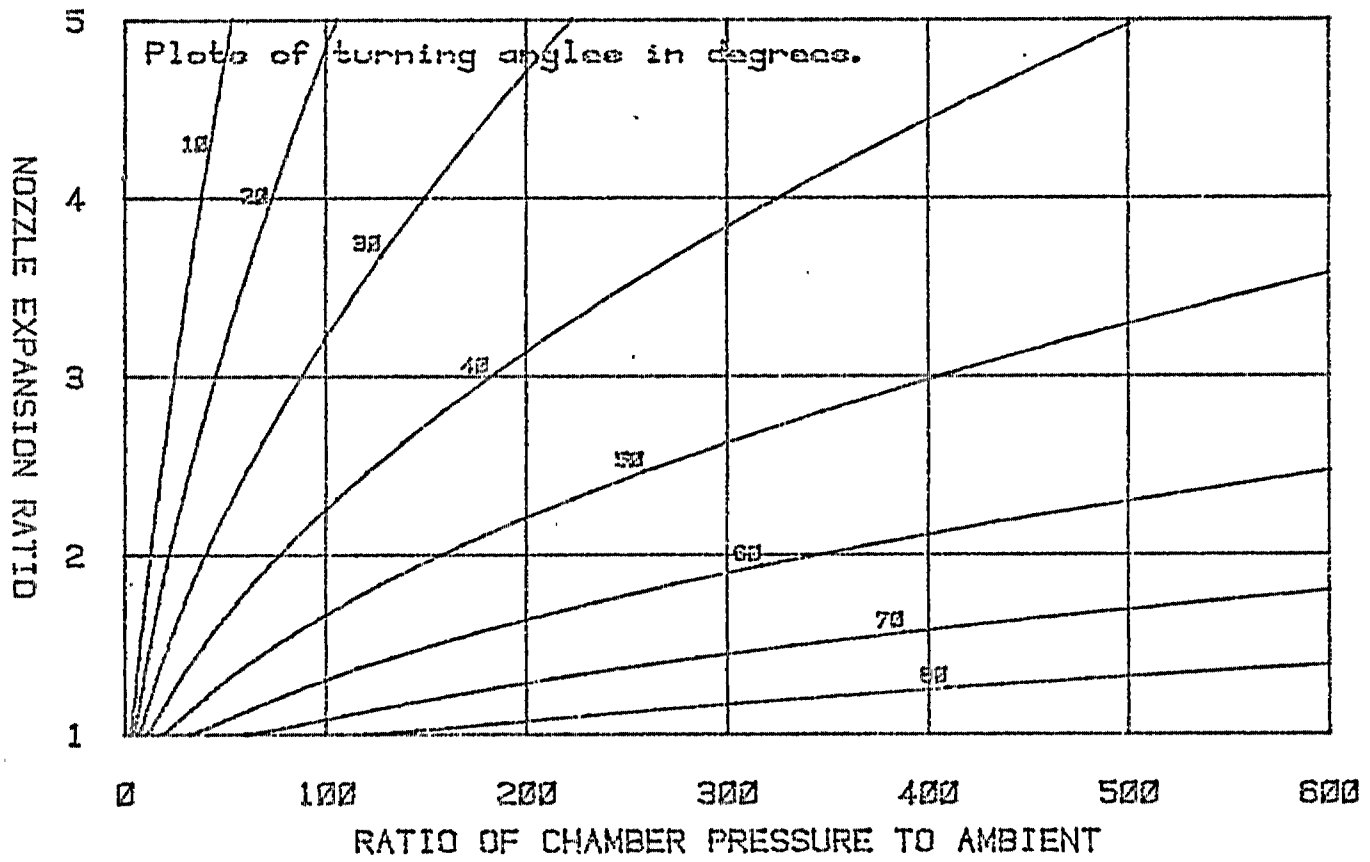

Figure 3.9(a) - Lines of constant nozzle lip turning angles plotted in the Pressure Ratio/Expansion Ratio plane for k=1.16.

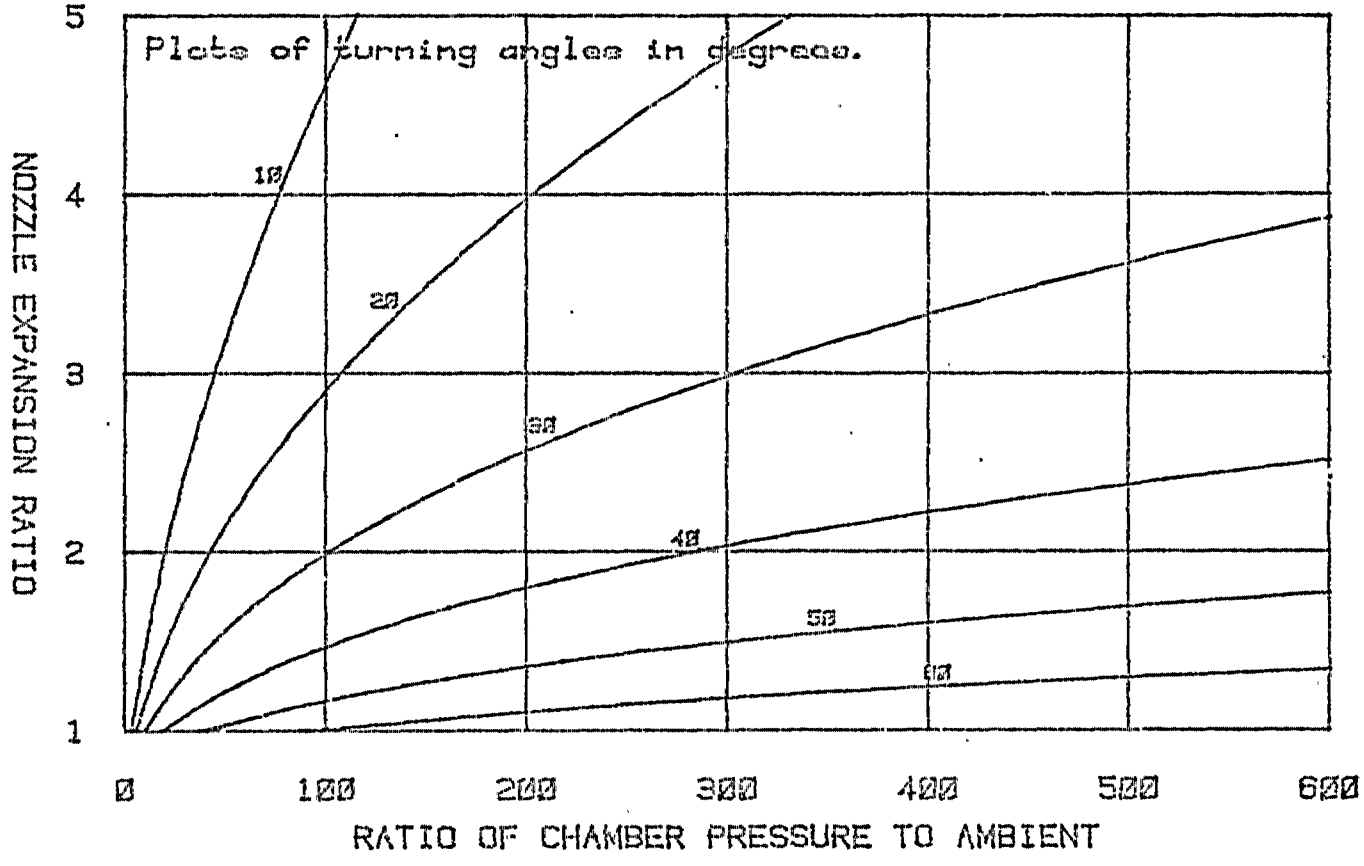

Figure 3.9(b) - Lines of constant nozzle lip turning angles plotted in the Pressure Ratio/Expansion Ratio plane for k=1.4.

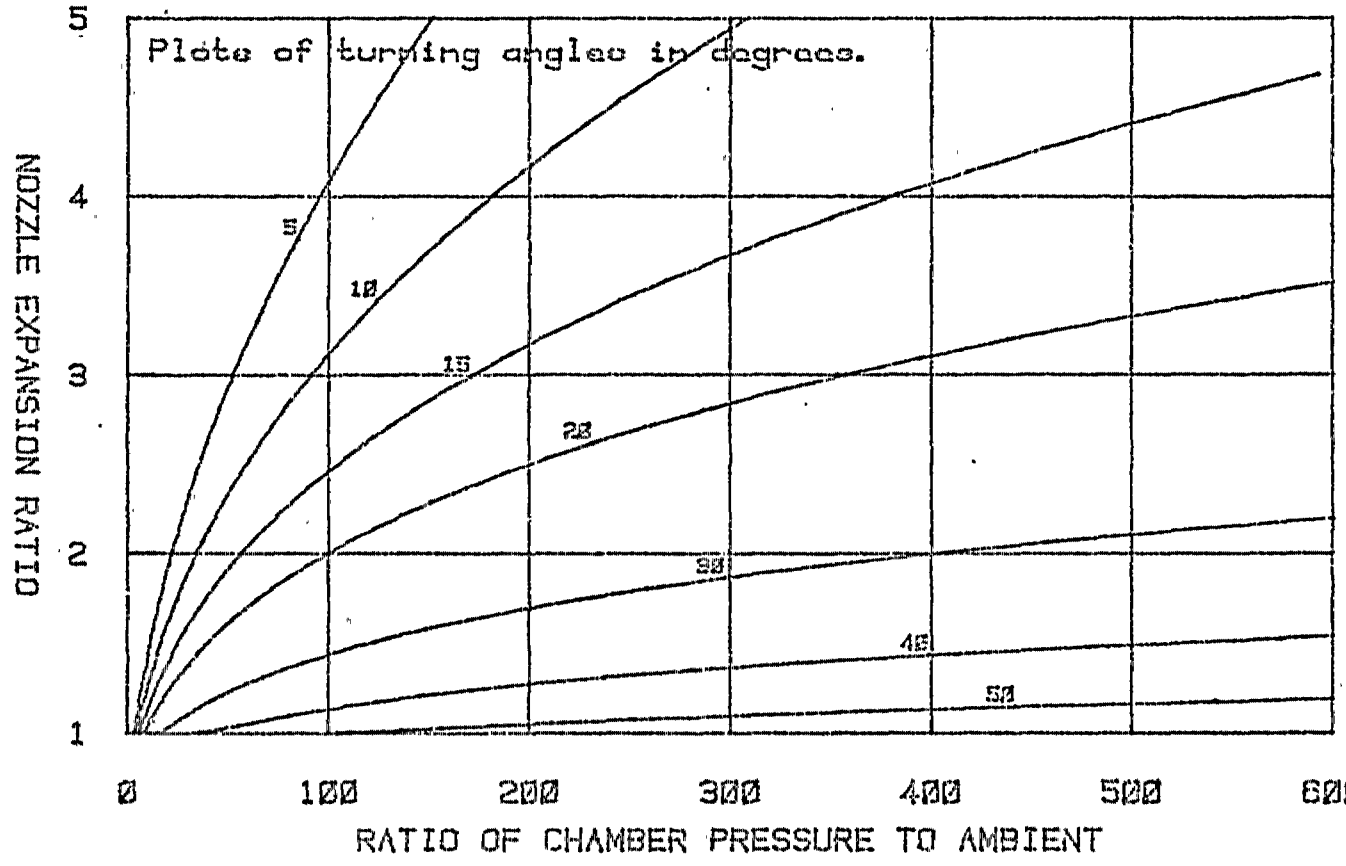

Figure 3.9(c) - Lines of constant nozzle lip turning angles plotted in the Pressure Ratio/Expansion Ratio plane for k=1.67.

SECTION 4

MODEL RESTRICTIONS

This section discusses conditions in which the model of this paper may underestimate the extent of the debris hazard area. Such conditions can arise when the input parameters of the model do not adequately describe the particles or the jet. The following paragraphs will discuss the effects of particle shape, obstructions, and external burning.

It is assumed in the model that a particle of debris is completely specified by its mass, projected area, and drag coefficient. This description may be inadequate for some classes of particle shapes. Particles with one very long or very short dimension (such as a length of wire or a thin disc) can develop lift and drag forces far more complex than those of the simple model assumed here. Particles with protruding points or edges may have penetrating powers well in excess of that suggested by Lewis' (1978) model.

As noted in the preceeding section, drag coefficient is a critical parameter in the model. Unfortunately, it is a parameter difficult to estimate for particles of irregular shape. A problem can arise if a particle presents a large area, high drag coefficient facet to the jet flow, but reorients itself and presents a small area, small

drag coefficient facet for its motion through the still air. Such a particle can have a greater range than a similar one described by a single drag coefficient. Equation (2.24), giving the minimum safe standoff distance, can be rederived keeping drag coefficients and projected areas separate for different phases of particle flight. In that case,

$$S > \frac{m}{2C_{da}A_a\rho_A}\left[\ln\left(\frac{2LC_{dj}A_jP_o}{Q_pA_p}\right) + \frac{\ln k}{k-1}\right] + L \qquad (4.1)$$

where C_{dj} and A_j are drag coefficient and projected are for motion in the jet, C_{da} and A_a for motion in the still air, and A_p is the projected area pertinent to particle impact. Equation (4.1) is probably of academic concern only, since, for a given class of particle, the semi-empirical constant L can absorb the differences in drag coefficients and projected areas.

Lift forces act perpendicularly to a particle's relative wind, and can serve to increase the angular dispersion of debris from a rocket backblast. (Baker (1978) discusses a lift induced range increase for debris from explosions. This can occur if lift forces are so oriented as to flatten a particle's trajectory. Small particles, as might be expected in a small rocket backblast, will slow to safe speeds before the range lengthening effects of lift can be felt. In any case, the model of this paper assumes the worst case condition of no trajectory curvature.)

The angular dispersion model of this paper is conservative in the sense that it will overestimate particle dispersion in the absence of lift. Careful consideration of fluid mechanics will reveal that a particle moving at the maximum predicted angular deflection will have received zero momentum in that direction. This should insure an adequate margin of safety for irregularly shaped particles. A thin, flat object, however, can literally fly out of the predicted region of hazard in a highly unpredictable fashion. If such objects--nozzle diaphrams or end caps, for example--are expected to be present in the debris, they should be considered to present a 360^{o} hazard until testing proves otherwise. The reader is reminded that a boomerang can readily negotiate a 720^{o} turn while maintaining enough momentum to inflict appreciable damage.

It is assumed in the model that the region behind the rocket is clear. Obstructions in the predicted region of debris hazard can deflect debris either directly through ricochet or indirectly through jet deflection or spalling. Ricochet can be expected to increase particle dispersion, possibly to the point of endangering the gunner. Frangible objects within a few jet wavelengths of the rocket nozzle may not only deflect debris, but may break up and themselves become part of the debris hazard. Again, these effects are situation dependent and likely to be unpredictable.

Particle range is unlikely to be much affected. Particle dispersion can be expanded to 360^{o} if there are solid obstructions in the near field.

It has been assumed that the rocket's jet is an adiabatic process, that is, that any combustion occurs within the rocket. The jet geometry may be altered if afterburning, or combustion external to the rocket, takes place. An extreme example of this is the afterburn explosion, which may occur when substantial amounts of unburned propellant accumulate in the plume before igniting. Afterburning in tactical rockets has been studied for many years (JANNAF, 1976). It is a highly complex phenomenom, depending on the interaction of propellant chemistry, ambient conditions, and fluid dynamics. Much is as yet poorly understood.

In general, one can expect afterburning to increase both the range and dispersion of backblast debris. The increase in range is likely to be small for two reasons. First, energy release in an afterburn is probably only a fraction of the energy release in a rocket's combustion chamber. Second, debris range for small rockets is relatively insensitive to changes jet plume characteristics. This is true for that same reason that standoff distance varies only slowly with L over the range of interest (see figure (3.7)). Dispersion, on the other hand, may be greatly increased, particularly in the event of an afterburn explosion. An afterburn explosion can increase

dispersion in at least two ways: it can deflect particles already accelerated in the main jet, and it can itself accelerate particles. The nature of these explosions is not understood, either analytically or empirically, to an extent that would allow reliable estimates to be made for dispersion from a given rocket. If afterburning is expected to occur in a given system, tests should be designed to detect debris with anomolously large dispersion angles. In the Viper test program, for example, particles of desicant have been caught on collection panels placed at the gunner's position (Chipser). Presumably, those particles were blown forward by energetic events occurring behind the launch tube.

While the debris hazard model has not yet been verified quantitatively against experiment, some qualitative observations were made during test firings of LAW and Viper at the Redstone Arsenal during 1980. Both of these weapons are shoulder-fired, tube launched antitank rockets of the sort for which the model is designed. Viper is described in more detail in Appendix C.

We were able to introduce 4 and 16 grain steel cubes into the backblast of one LAW firing. Those cubes, similar to those used by Lewis (1978), were glued to vellum paper stretched across the breech of the launch tube. Witness panels, consisting of two inches of foamed plastic backed by half an inch of plywood, were placed at ten

meters and twenty meters directly behind the LAW. A streak camera was set up to record particle velocities approximately one half meter behind the launch tube breech. Three cubes were recovered after firing--two from the plywood of the ten meter panel and one from the plywood of the twenty meter panel. There was also a hole through the ten meter panel where an object, presumably a cube, had penetrated. A number of dense streaks were recorded by the camera, corresponding to particles moving to the rear between 150 and 450 meters per second. There is no way to determine whether any of the streaks were caused by cubes. Additionally, there was one streak which would have been caused by a particle moving forward from some place to the rear of the LAW with a velocity of approximately 200 meters per second. We have speculated that this may have been a particle propelled by an afterburn explosion. The witness panels have never been calibrated to correlate particle penetration to particle velocity or to skin penetration. It was noted, however, that the steel cubes had more penetrating power than other, less dense, debris from the rocket motor. This qualitative observation is in agreement with the prediction of the model.

From the Viper tests, we have some witness panel observations and some debris distribution observations.

Again, these observations are qualitative, since the experiments were uncontrolled and uncalibrated with regard to debris hazard. The debris consisted of irregular plastic "detente fingers" about a centimeter long, pieces of wiring and ignitors, fragments of the plastic nozzle closure ranging in size to the full disc, styrofoam throat plugs, and so forth. There was a great deal of variation in the rocket configuration from test to test.

Witness panels as described above were placed at ten and twenty meters on some runs and at the gunner's position on at least one set of runs. As might be expected, particle penetration on the ten meter panel was generally greater than on the twenty meter panel. There have been some measurements made of penetration depth and particle characteristics, which may be useful if someone ever calibrates the panels. While the gunner's position panel was intended to pick up debris thrown backward as the rocket exited the launch tube, it also picked up desicant spheres (about one mm diameter) on the rear facing side (Chipser, 1980). Again, we speculate that this was debris blown forward by an afterburn explosion.

Debris dispersion can be estimated from the distribution of launch site ground debris. After a number of firings of both LAW and Viper, there was a good deal of debris found along lines extending backwards from the launch tube breech at about forty-five degrees off axis. Very little debris was found more than sixty degrees off axis.

While these observations are substantially in agreement with the model predictions (see Section 3), we stress their qualitative nature. The firings were uncontrolled experiments in this regard, and personal activity in the launch site vicinity would have redistributed the debris to some extent. John Chipser (1980) of the Human Engineering Laboratory has noted that the witness panels collect a surprisingly small amount of debris at their standard on axis locations. He has recommended that the panels be moved off axis, noting that debris concentration is heaviest along the aforementioned forty-five degree lines. Such experiments are as yet pending.

SECTION 5

CONCLUSIONS

The preceeding sections have developed a model for backblast debris hazard from small rockets. The model itself represents a balance between plausible physics and useable engineering. Verification of the model against real world experiments remains yet to be accomplished.

Physics of the model are covered in Section 2; use of the model is covered in Sections 3 and 4. Sections 3 and 4 amount to "how to do it" sections, and can be read independently of Section 2. We believe that this format maximizes accessibility to potential users, but we caution against the blind use of any semiempirical model. The computer codes, of course, can be used without any understanding of the physics.

It is important that the model be given quantitative verification in experiments designed expressly for that purpose. Verification of this essentially stochastic model will require many shots fired under calibrated and controlled conditions. Our difficulties with "piggybacking" on the Viper test program lead us to believe that programs where conditions are determined by other experiments are apt to be wasteful.

REFERENCES

1. W. E. Baker, J. J. Kulesz, R. E. Ricker, P. S. Westine, V. B. Parr, L. M. Vargas, P. K. Mosely; "Workbook for Estimating Effects of Accidental Explosions in Propellant Ground Handling and Transport Systems", NASA-CR-3023 (Aug. 1978).

2. C. Che-Haing, "Axially Symmetric Supersonic Turbulent Jets Discharged from a Nozzle with Underexpansion", in Turbulent Jets of Air, Plasma, and Real Gas, edited by G. N. Abramovich; Consultants Bureau, a Division of Plenum Pub. Corp., N.Y. (1969).

3. J. Chipser, Personal communication, Viper Project Office, Redstone Arsenal, Huntsville, AL (1980).

4. JANNAF Handbook, Rocket Exhaust Plume Technology, Chapter 2: Fluid Dynamic Flow Models (1976).

5. J. S. deKrasinsky, "Comments on Research Report IV-23", in Second U.S. National Conference on Wind Engineering Research, Proceedings, Colorado State Univ., Ft. Collins, Colorado (1975), p. IV-33-1.

6. C. H. Lewis, Jr., D. J. Carlson, "Normal Shock Location in Underexpanded Sonic Jet", AIAA Journal, vol. 2, n. 4 (Jan. 1968), p.776.

7. J. H. Lewis, P. A. Coon, V. R. Clare, L. M. Sturdivan, "An Empirical/Mathematical Model to Estimate the Probability of Skin Penetration by Various Projectiles", ARCSL-TR-78004 (April 1978).

8. E. S. Love, C. E. Grigsby, L. P. Lee, M. J. Woodling, "Experimental and Theoretical Studies of Axisymmetric Free Jets", NASA-TR-R-6 (1959).

9. W. Z. Sadeh, "Drag of Tornado-Generated Missiles", in Second U.S. National Conference on Wind Engineering Research, Proceedings, Colorado State Univ., Ft. Collins, Colorado (1975), p. IV-31-1.

10. E. M. Schmidt, D. D. Shear, "The Flow Field about the Muzzle of an M-16 Rifle", BRL-R-1692 (Jan. 1974).

11. A. H. Shapiro, The Dynamics and Thermodynamics of Compressible Fluid Flow, vol. I, p. 466, Ronald Press Co., N.Y. (1953).

12. G. J. Van Wylen, Thermodynamics, Ch. 13, John Wiley & Sons, Inc., N.Y. (1959).

13. S. H. Walker, D. B. Duncan, "Estimation of the Probability of an Event as a Function of Several Independent Variables", Biometrica, V. 54, p. 167 (1967).

APPENDIX A

JET PLUME STRUCTURE

This appendix presents an overview of jet plume structure pertinent to the debris hazard problem. The descriptions will be generally qualitative with references given to quantitative analyses where needed. Of primary importance for the debris hazard model is the extent of the bottle shock region. An empirical relation will be given for this. Additionally, some basic properties of a tube confined supersonic flow will be discussed.

Underexpanded supersonic jets have complex structures that have so far defied any simple explanations. The method of characteristics (Shapiro, 1953) and an assortment of hydrocodes (JANNAF, 1976) have all been used in the last twenty or thirty years to map out velocity and pressure flow fields in such jets. Concurrently, jets have been probed and photographed over a wide range of physical conditions. The enormity of the problem is underscored by the fact that, under tremendous impetous from the missile development programs, theory and experiment are only beginning to come into good agreement.

Figure (A1) illustrates the bottle shock region of a steady, underexpanded, supersonic jet. At the exit

plane, the jet has a Mach number of M_E and a pressure of P_E. It expands into still air with a smaller pressure of P_A.

For now, assume the flow is of a perfect gas with no heat addition. In that case, there will be a Prandtl-Meyer expansion fan attached to the nozzle lip. This is illustrated in the upper portion of figure (A1). The lines of the fan represent characteristics across which fluid thermodynamic properties change by some fixed factor. As it crosses these characteristics, the gas turns away from the jet axis and drops in pressure, so that a diverging source type flow is developed in the vicinity of the nozzle. The innermost characteristic can be interpreted as the disturbance from the nozzle lip propagating into the jet. This disturbance propagates inward at the Mach angle.

It is the diverging nature of the flow that eventually leads to computational problems. Gas in a diverging supersonic flow must continuously drop in pressure, but the outer boundary of the jet is held at atmospheric pressure. The apparent paradox is resolved in the flow when the expansion fan reflects from the surface of specified pressure which marks the jet's boundary. (For inviscid fluids, that boundary is a vortex sheet, that is, a velocity discontinuity.) The reflection changes the sense of the expansion waves in that they become compression waves with opposite their

original turning angles. Problems arise when this system of compression waves coalesce to form an oblique shock imbedded in the plume. This shock, because of its shape, is referred to as a bottle shock. Gas within the bottle shock remains in a divergent compressible source flow. At the shock, it turns sharply downstream and forms a lower speed, though still supersonic, sheath between the bottle shock and the ambient air.

Further complications arise downstream, since the barrel shock bends around and reflects from the jet axis. For overpressure ratios greater than about 2, this is generally a Mach reflection (Love, 1959), with a Mach stem extending from the barrel shock towards the axis to form a so-called Mach disc (or Rieman wave in plane jets). As the Mach disc can be of enormous strength and so drastically alter the fluid motion, its location is of great importance in describing the jet -- many features of the jet scale on the primary wavelength, i.e. the distance to the Mach disc.

The primary wavelength can be calculated (sometimes!) with hydrocodes or with any of a number of empirical formulas. It is a function of Mach number and ratio of specific heats, and, to a lesser extent, of nozzle divergence, combustion chemistry, and particulate loading. Lewis (1966) gives the relationship

$$\frac{\lambda}{d} = .69\ M_E \left(\frac{kP_E}{P_A}\right)^{\frac{1}{2}} \cdot \left(1 + 0.197\ M_E^{1.45}\ \phi^{0.6}\right)^{-1} \qquad (A.1)$$

where d is nozzle diameter, M_E is Mach number at nozzle exit, P_E is pressure at nozzle exit, P_A is ambient pressure, and ϕ is fractional particulate mass density. Lewis notes that this fits his data to within five percent, but that there is considerable scatter between data from different investigations.

Beyond the Mach disc, the flow takes on an annular form. Gas passing through the Mach disc is shocked subsonic, leaving a subsonic core flow surrounded by a supersonic sheath. Virtually all the momentum flux is carried in this sheath. Viscous and turbulent processes transport momentum from the sheath and into the core and the ambient atmosphere. Che-Haing (1969) has treated these processes semiempirically, but the results are difficult to use. As a general rule, velocities in the jet beyond the Mach disc decay roughly as the inverse of the downstream position (JANNAF, 1976). This occurs as momentum is transferred, primarily through turbulent mixing, to the ambient air.

An impulsive starting flow for a supersonic jet is a highly complex phenomenon. In general, there will be a supersonic region extending from the nozzle. Schlieren photographs (Schmidt, 1974) show this region to resemble closely a truncation of the corresponding fully developed flow. At the downstream end of this region there will be an expanding recirculation zone which entrains ambient air and interfaces jet momentum

flux to the atmosphere. There is frequently a well defined vortex ring generated by this process. Finally, the expanding gases will generate compression waves in the ambient air which can be expected to form one or more spherical shocks.

A tube confined supersonic jet can be profoundly different from a free jet. Scaling in such a flow depends not only on rocket exit conditions, but also on the relative size of the tube, on the distance to the tube exit, and on the characteristics of the tube wall. In tube launched weapons, the rocket nozzle exit diameter is probably not much smaller than the inside diameter of the tube. Three cases can be delineated according to the distance the rocket is placed from the end of the tube.

For a nozzle position very close to the tube exit, the jet is virtually unaffected. If a line drawn downstream from the nozzle lip at the maximum streamline divergence angle (see Section 2) does not intercept the tube, then this condition is satisfied.

For nozzle positions up to a diameter or so from the tube exit, the tube can act much as an extension of the nozzle. "Exit" conditions can be referred to the tube exit as opposed to the rocket nozzle exit. Debris dispersion angle is likely to be reduced since the overpressure ratio measured at the tube exit is smaller than the overpressure ratio measured at the nozzle exit of the unconfined rocket.

For nozzle positions further than a diameter from the tube end, there can be a substantial boundary layer build up and internal shocking inside the tube. These phenomena depend critically on tube roughness and on the nature of the jet itself. Conditions at the tube exit are best found empirically in this case. Once those conditions are known, the nature of the external plume can be estimated by previously outlined procedures. It is important to the debris hazard problem that the pressure at the tube exit in this case can be larger than the pressure at the nozzle exit of the unconfined rocket. Contrary to intuition, extending the breech of a rocket launch tube has the potential of increasing debris dispersion angle.

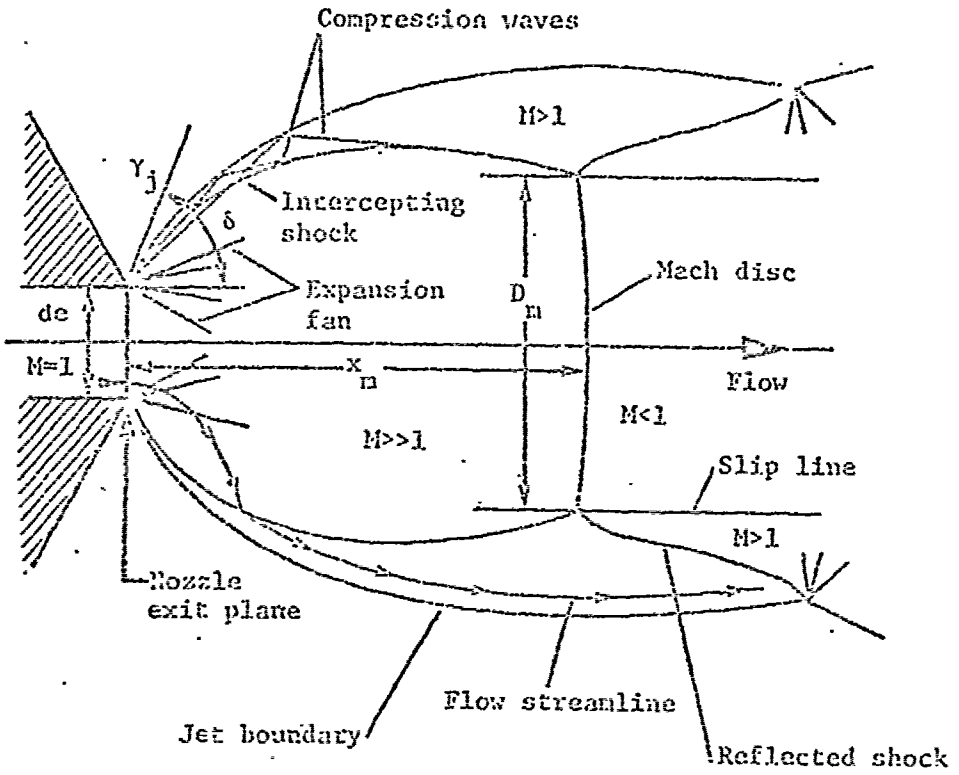

Figure A.1 - Diagram of bottle shock region of an underexpanded, supersonic jet. This figure is taken from the JANNAF Handbook, Rocket Exhaust Plume Technology, p.2-4-13.

APPENDIX B

PENETRATION OF SKIN BY BALLISTIC PARTICLES

Lewis (1978) has developed a semiempirical model for estimating the probability of skin penetration by high speed debris. A series of experiments, in which objects were thrown against simulated skin/clothing combinations, was used to calibrate the model. The objects included tungsten and steel cubes, wooden cylinders, and gravel; their masses were typically between a quarter gram and four grams. Three skin/clothing combinations were investigated, simulating bare skin, summer weight uniform, and winter weight uniform. Lewis' report contains extensive tables of the experiment results. The model is presented here in a somewhat modified form.

It can be reasoned that skin penetration must be a function of particle dynamics and geometry and of target material properties. For geometrically similar particles and homogeneous target material, a model must certainly include a particle characteristic length D, particle mass m, particle velocity v, and an areal toughness T. (Areal toughness is defined as the amount of mechanical energy that can be absorbed per unit area of a thin material before fracture occurs. It has units of energy per length squared.) These parameters can be combined to form a dimensionless group Π

$$\Pi = \frac{Mv^2}{D^2T} \qquad \text{(B1)}$$

Π is evidently a measure of the kinetic energy delivered per unit area of target divided by the target areal toughness. We expect that for Π large enough, the mechanical energy deposited in the target exceeds the target's capacity to absorb energy without fracture.

In general, the particle is irregular and tumbling, and the target is inhomogeneous, anisotropic, and rate dependent. Neglecting these factors will result in an apparent scatter of the penetration data. For example, if the particle is a tumbling cube, there may well be a range for Π in which penetration occurs when the cube impacts with a corner, but does not occur when the cube impacts with a flat. A probabilistic model is then appropriate:

$$p\{\text{skin penetration}\} = f(\Pi) \qquad \text{(B2)}$$

where p{E} is the probability density function for occurance of event E.

Lewis has fitted S curves to his data using the Walker-Duncan method (Walker, 1967). He uses the particle's projected area A instead of D^2. These curves are replotted in figure (B1). The ordinate is the natural logarithm of the numerical value of $\frac{mv^2}{A}$ in SI units. (Note that Lewis uses a system of mixed units.) As a result, a different curve is obtained for each value of T, that is, for each skin/clothing configuration. The 50% probability level is summarized in table (B1).

TABLE B.1

50% Skin Penetration Parameters

Skin/Clothing	$Q_p = \frac{m_p v^2}{A_p}$
bare skin	150,000 $\frac{kg}{sec^2}$
2 layer uniform (summer weight)	340,000 $\frac{kg}{sec^2}$
6 layer uniform (winter weight)	739,000 $\frac{kg}{sec^2}$

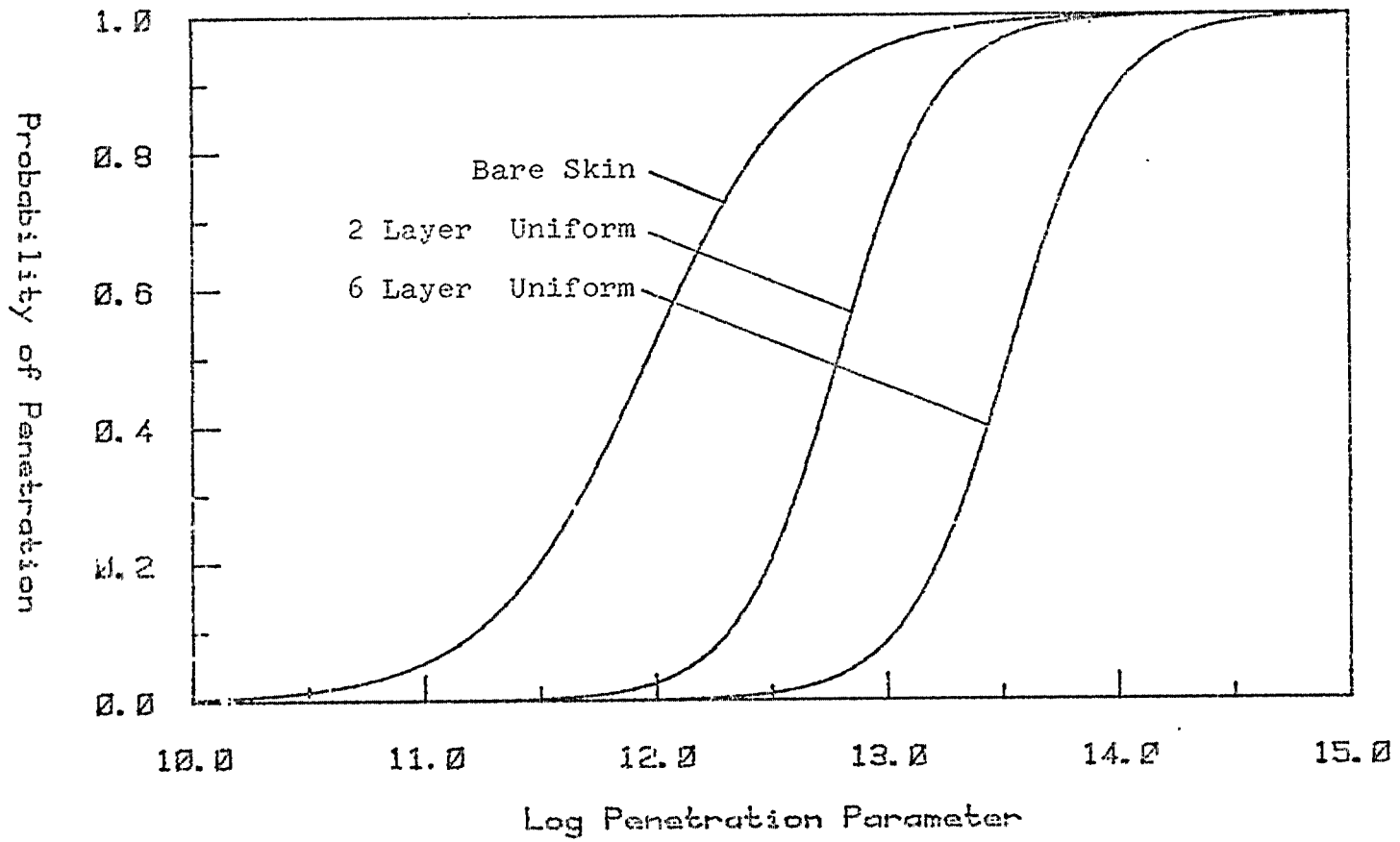

Figure B.1 - Plot of probability of skin penetration versus the natural log of the numerical value of $\frac{mv^2}{A}$ in SI units.

APPENDIX C

VIPER CHARACTERISTICS

The Viper is a shoulder launched light anti-tank rocket under development by General Dynamics. The motor, using a high performance boron based propellent, burns out within the launch tube. Data given below apply to a configuration tested in the spring of 1980, and may not be representative of current design. They are pre ented to illustrate the sort of data necessary to use the debris hazard model.

TABLE C.1

VIPER CHARACTERISTICS

PARAMETER	SYMBOL	VALUE FOR VIPER
Rocket Motor:		
Nozzle exit diameter	d_E	0.0424m
Nozzle throat diameter	d^*	0.0616m
Nozzle divergence angle	θ_N	11^o
Chamber pressure	P_o	6.8×10^7 N/m^2
Specific heat ratio for combustion products	k	1.16
Debris (plastic detente fingers used to secure rocket in launch tube):		
Projected area	A_p	10^{-4} m^2
Mass	m	7×10^{-4} kg
Drag coefficient	C_d	0.5
Target (summer weight uniform - two layers of clothing):		
Skin penetration parameter	Q_p	3.4×10^5 kg/sec^2
Ambient air (sea level, 25^oC):		
Mass density	ρ_A	1.29 kg/m^3
Pressure	P_A	10^5 N/m^2

APPENDIX D

COMPUTER AND CALCULATOR CODES

Two codes are given here which implement the debris hazard model as developed in Section 2. The first code is written in floating point BASIC and should run on any machine supporting that language. The second code is written for the Hewlett-Packard 41C programmable calculator and is specific to that device. The algorithms used in these codes are discussed in Program Notes sections, and can be adapted to other languages.

BACKBLAST DEBRIS HAZARD CODE

IN BASIC

PROGRAM NOTES:

This code is documented by remarks contained in the listing. Note that the listing appearing in this appendix is for SI units. To run the code, type RUN. The code will interogate for pertinent physical parameters. A sample session, run on the University of Tennessee Space Institute VAX-11, follows the listing; the file containing the listing was named DEB2.BAS.

PROGRAM LISTING:

```
10 REM--          DEBRIS HAZARD AREA FOR ROCKET BACKBLAST
20 REM--   This program calculates the dimensions of a circular sector
30 REM--to the rear of a rocket in which there is a debris hazard.
40 REM--Input is in three sections: one specifying the rocket, one
50 REM--specifying object or person to be protected, and one describing
60 REM--the debris.  The program is designed to be run in MKS units,
70 REM--but can be changed to any other system of consistent units
80 REM--by changing the air constants in statements 330 and 340.
90 PRINT "ROCKET DATA"
100 INPUT "   Nozzle throat diam: ",Dnt
110 INPUT "     Nozzle exit diam: ",Dne
120 INPUT "     Chamber pressure: ",Pc
130 INPUT "  Specific heat ratio: ",K
140 INPUT "    Nozzle half angle: ",Nozang
150 PRINT "SKIN PENETRATION PARAMETER"
160 REM--G is a measure of energy per volume required to fracture
170 REM--target material.  In MKS units the following values
180 REM--can be used (see J.H.Lewis et al,'An Empirical/Mathematical
190 REM--Model to Estimate the Probability of Skin Penetration by
200 REM--Various Projectiles', AECSL-TR-78004, Apr 78.
210 REM --          bare skin----------G=150000 kJ/sec*sec
220 REM --          2 layer uniform---G=340000 kJ/sec*sec
230 REM--           6 layer uniform---G=730000 kJ/sec*sec
```

```
240 INPUT "                          R: ",R
250 PRINT "DEBRIS DATA  (enter 0 to exit)"
260 INPUT "       Projected area: ",Ap
270 REM--Exit program if 0 assigned to Ap.
280 IF Ap=0 THEN GOTO 780
290 INPUT "                    Mass: ",Mp
300 INPUT "     Drag coefficient: ",Cd
310 REM--Rhoair=density of air in kilograms per cubic meter
320 REM--Pair=pressure of air in newtons per square meter
330 Rhoair=1.2929
340 Pair=100000
350 REM--Lmult is the number of jet primary wavelengths over which
360 REM-- significant particle acceleration occurs.  Experiments
370 REM-- may suggest that a value other than 1 is more appropriate.
380 Lmult=1
390 REM--K1,K2,K3 are internal constants for programming convenience.
400 K1=(K+1)/(K-1)
410 K2=2/(K-1)
420 K3=2*(K-1)/(K+1)
430 REM--Aratio is the nozzle's exit to throat area ratio.
440 Aratio=(Dne/Dnt)^2
450 REM--The next five statements calculate exit Mach number, Mexit.
460 REM-- Mach is a dummy variable used for temporary storage.
470 Mach=1
480 Mexit=Mach
490 Mach=SQR(K1*(Aratio-1/Mexit^K3-K2)
500 IF ABS(Mach-Mexit)>.01 THEN GOTO 480
510 Mexit=Mach
520 REM--Calculate exit plane pressure, Pexit
530 Pexit=Pc*(1+.5*(K-1)*(Mexit^2))^(K/(1-K))
540 REM--Calculate jet primary wavelength, Wavel, using Lewis' formula.
550 Wavel=.69*Dne*Mexit*SQR(K*Pexit/Pair)
560 REM--Calculate particle acceleration distance, L
570 L=Wavel*Lmult
580 REM--Internal variables.
590 Parm1=.5*Mp/(Cd*Ap*Rhoair)
600 Parm2=LOG(2*L*Cd*Pc/R)
610 REM--Calculate minimum safe standoff distance.
620 Standoff=Parm1*(Parm2+LOG(K)/(K-1))+L
630 PRINT "   Minimum safe standoff distance = ",Standoff
640 REM--Remainder of program calculates dispersion half angle.
650 REM--Calculate maximum Mach number on jet boundary.
660 Mair=SQR(K2*((Pc/Pair)^((K-1)/K)-1))
670 REM--Calculate Prandtl-Meyer turning angle for Mexit.
680 Parm3=Mexit^2-1
690 Angle1=SQR(K1)*ATN(SQR(Parm3/K1))-ATN(SQR(Parm3))
700 REM--Calculate Prandtl-Meyer turning angle for Mair.
710 Parm3=Mair^2-1
720 Angle2=SQR(K1)*ATN(SQR(Parm3/K1))-ATN(SQR(Parm3))
730 REM--Calculate dispersion half angle, Disband, in degrees.
740 Disband=57.3*(Angle2-Angle1)+Aband
750 PRINT "   Dispersion up to ",Disband," degrees"
760 PRINT " "
770 GOTO 250
780 END
```

Figure E.1 - Example session of BASIC debris hazard code.

```
  BASIC

VAX-11 BASIC V1.0

Ready

OLD DEBR.BAS
Ready

RUN
DE32            5-DEC-1980 17:18

ROCKET DATA
    Nozzle throat diam:       ? .0424
      Nozzle exit diam:       ? .0616
      Chamber pressure:       ? 68000000
  Specific heat ratio:        ? 1.16
     Nozzle half angle:       ? 11
SKIN PENETRATION PARAMETER
                        Q:    ? 340000
DEBRIS DATA  (enter 0 to exit)
        Projected area:       ? .0001
                  Mass:       ? .0007
      Drag coefficient:       ? .5
   Minimum safe standoff distance =          33.6709
   Dispersion up to             77.3552      degrees

DEBRIS DATA  (enter 0 to exit)
        Projected area:       ? 0
Ready
```

BACKBLAST DEBRIS HAZARD CODE FOR

HP-41C PROGRAMMABLE CALCULATOR

PROGRAM NOTES:

This code requires 63 registers of program memory and 15 registers of storage memory. Running the code puts the calculator into degrees mode, fixes the display at zero digits, and sets flag Ø1.

Lines ØØ1 through Ø34 are for input; line Ø25 is an entry point for debris specification. Lines Ø37 through Ø68 solve equation (2.22) for Mach number as a function of area ratio; M_E remains in register Ø15 after the program runs. Lines Ø7Ø through Ø95 calculate the jet wavelength and store it in register Ø3; λ remains in that register after the program runs. Lines Ø97 through 124 calculate the standoff distance. Lines 127 through 146 calculate the dispersion angle θ_{max}. Lines 147 through 154 display standoff distance and maximum dispersion angle. Line 156 loops to additional debris input. Lines 157 through 174 are a subroutine for calculating the Prandtl-Meyer turning angle, equation (2.31), given Mach number.

The code is set up to handle multiple debris specifications consecutively. After the first specification, flag Ø1 causes substantial portions of the code to be skipped.

PROGRAM USAGE

The listing below is designed for SI units and for standard atmosphere. Line ØØ5 has ambient air pressure of 100,000 N/m^2 and line 12Ø has ambient air density of 1.29 kg/m^3. The code can be set to other units or to other ambient conditions by changing the numerical constants on those two lines. Data entry must be in consistent units.

To run the code, load and press R/S. An example session is given in figure (E.2).

PROGRAM LISTING:

```
ØØ1  LBL "DEBRIS
ØØ2  CF  Ø1
ØØ3  DEG
ØØ4  FIX  Ø
ØØ5  1ØØØØØ
ØØ6  STO  Ø1
ØØ7  "THROAT DIAM
ØØ8  PROMPT
ØØ9  STO  Ø3
Ø1Ø  "EXIT DIAM
Ø11  PROMPT
Ø12  STO  Ø4
Ø13  "NOZZLE ∠
Ø14  PROMPT
Ø15  STO  Ø5
Ø16  "CHAMBER  P
Ø17  PROMPT
Ø18  STO  Ø6
Ø19  "GAMMA
Ø2Ø  PROMPT
Ø21  STO  Ø7
Ø22  "PENETRATION
Ø23  PROMPT
Ø24  STO  Ø8
Ø25  LBL  Ø1
Ø26  "DEBRIS AREA
Ø27  PROMPT
Ø28  STO  Ø9
Ø29  "DEBRIS MASS
Ø3Ø  PROMPT
```

```
Ø31   STO  1Ø
Ø32   "DRAG COEFF
Ø33   PROMPT
Ø34   STO  11
Ø35   FS?  Ø1
Ø36   GTO  Ø4
Ø37   RCL  Ø7
Ø38   RCL  Ø7
Ø39   1
Ø4Ø   ST + Z
Ø41   -
Ø42   1/X
Ø43   STO  12
Ø44   *
Ø45   STO  13
Ø46   2
Ø47   ST*  12
Ø48   1
Ø49   LBL  Ø2
Ø5Ø   STO Y
Ø51   SQRT
Ø52   RCL  Ø4
Ø53   RCL  Ø3
Ø54   /
Ø55   x^2
Ø56   *
Ø57   2
Ø58   RCL  13
Ø59   /
Ø6Ø   Y^X
Ø61   RCL  13
Ø62   *
Ø63   RCL  12
Ø64   -
Ø65   .001
Ø66   ST + Z
Ø67   RDN
Ø68   X>Y ?
Ø69   GTO  Ø2
Ø7Ø   STO  15
Ø71   RCL  12
Ø72   /
Ø73   1
Ø74   +
Ø75   RCL  Ø7
Ø76   RCL  12
Ø77   *
Ø78   CHS
Ø79   Y^X
Ø8Ø   SQRT
Ø81   RCL  Ø6
Ø82   *
Ø83   RCL  Ø7
Ø84   *
```

```
Ø85   RCL  Ø1
Ø86   /
Ø87   SQRT
Ø88   RCL  Ø4
Ø89   *
Ø9Ø   RCL  15
Ø91   SQRT
Ø92   *
Ø93   .69
Ø94   *
Ø95   STO  Ø3
Ø96   LBL  Ø4
Ø97   RCL  Ø3
Ø98   STO  Ø4
Ø99   RCL  11
1ØØ   *
1Ø1   RCL  Ø6
1Ø2   *
1Ø3   2
1Ø4   *
1Ø5   RCL  Ø8
1Ø6   /
1Ø7   LN
1Ø8   RCL  Ø7
1Ø9   SQRT
11Ø   LN
111   RCL  12
112   *
113   +
114   RCL  1Ø
115   *
116   RCL  11
117   /
118   RCL  Ø9
119   /
12Ø   1.29
121   /
122   2
123   /
124   ST + Ø4
125   FS?  Ø1
126   GTO  Ø6
127   SF   Ø1
128   RCL  Ø6
129   RCL  Ø1
13Ø   /
131   1
132   RCL  Ø7
133   1/x
134   -
135   Y^X
136   1
137   -
138   RCL  12
```

```
139   *
140   XEQ  Ø5
141   STO  14
142   RCL  15
143   XEQ  Ø5
144   ST - 14
145   RCL  Ø5
146   ST + 14
147   ᵀ, ∠=
148   ASTO Ø1
149   LBL  Ø6
150   ᵀD =
151   ARCL Ø4
152   ARCL Ø1
153   ARCL 14
154   AVIEW
155   STOP
156   GTO  Ø1
157   LBL  Ø5
158   1
159   -
160   SQRT
161   STO  Ø2
162   RCL  13
163   SQRT
164   /
165   ATAN
166   RCL  13
167   SQRT
168   *
169   RCL  Ø2
170   ATAN
171   -
172   RCL  Ø5
173   +
174   RTN
175   END
```

Figure (E.2). Example session of HP-41C Debris Hazard Code.

USER ACTION	DISPLAY	REMARKS
R/S	THROAT DIAM	Enter nozzle throat diameter, d*
.0424	.0424	d* in meters
R/S	EXIT DIAM	Enter nozzle exit diameter, d_E
.0616	.0616	d_E in meters
R/S	NOZZLE ∠	Enter nozzle divergence angle θ_N
11	11	θ_N in degrees
R/S	CHAMBER P	Enter chamber pressure P_o
68000000	68,000,000	P_o in N/m^2
R/S	GAMMA	Enter specific heat ratio k of exhaust products
1.16	1.16	
R/S	PENETRATION	Enter penetration parameter Q_p
340000	340,000	Q_p in kg/s^2
R/S	DEBRIS AREA	Enter particle's projected area A
.0001	.0001	A in m^2
R/S	DEBRIS MASS	Enter particle's mass m
.0007	.0007	m in kg
R/S	DRAG COEFF	Enter particle's drag coefficient C_d
.5	.5	

Figure (E.2) continued

USER ACTION	DISPLAY	REMARKS
R/S	D=34., L=77.	Standoff distance D in m, dispersion angle L in degrees. Execution takes about 15 seconds.
R/S	DEBRIS AREA	Loops for additional debris input.

APPENDIX E

SOLUTION OF EQUATION (2.22)

Equation (2.22) gives area ratio as a function of Mach number:

$$\frac{A_E}{A^*} = \frac{1}{M_E}\left[\left(\frac{2}{k+1}\right)\left(1 - \frac{k-1}{2} M_E^2\right)\right]^{\frac{(k+1)}{2(k-1)}} \qquad (2.22)$$

The model requires Mach number as a function of area ratio. The inversion can be accomplished by iteration.

Reformulate equation (2.22) to read:

$$M_E = \left[\left(\frac{k+1}{k-1}\right)\left(\frac{A_E}{A^* M_E}\right)^{\frac{2(k-1)}{(k+1)}} - \frac{2}{k-1}\right]^{\frac{1}{2}} \qquad (E.1)$$

Assume a trial Mach number of unity and evaluate the right hand side of equation (E.1). Take this value as an updated trial Mach number and repeat the procedure. Satisfactory convergence will generally occur in four or five iterations. See also figure (3.3).